Available at www.sciencedirect.com

ScienceDirect

journal homepage: www.elsevier.com/locate/he

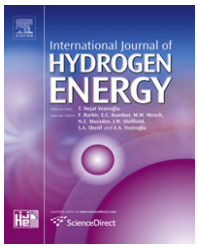

Canada's program on nuclear hydrogen production and the thermochemical Cu–Cl cycle

G.F. Naterer [a,*], S. Suppiah [b], L. Stolberg [b], M. Lewis [c], Z. Wang [a], V. Daggupati [a], K. Gabriel [a], I. Dincer [a], M.A. Rosen [a], P. Spekkens [d], S.N. Lvov [e], M. Fowler [f], P. Tremaine [g], J. Mostaghimi [h], E.B. Easton [a], L. Trevani [a], G. Rizvi [a], B.M. Ikeda [a], M.H. Kaye [a], L. Lu [a], I. Pioro [a], W.R. Smith [a], E. Secnik [a], J. Jiang [i], J. Avsec [j]

[a] University of Ontario Institute of Technology (UOIT), 2000 Simcoe Street North, Oshawa, Ontario, Canada L1H 7K4
[b] Atomic Energy of Canada Limited (AECL), Chalk River, Ontario, Canada K0J 1J0
[c] Argonne National Laboratory, Chemical Engineering Division, 9700 S. Cass Avenue, Argonne, Illinois 60439, USA
[d] Ontario Power Generation (OPG), 889 Brock Road, Pickering, Ontario, Canada
[e] Pennsylvania State University, Department of Materials Science and Engineering, 207 Hosler Building, University Park, PA 16802, USA
[f] University of Waterloo, 200 University Ave., Waterloo, Ontario, Canada N2L 3G1
[g] University of Guelph, 50 Stone Road East, Guelph, Ontario, Canada N1G 2W1
[h] University of Toronto, Department of Mechanical and Industrial Engineering, Toronto, Ontario, Canada M5S 3E5
[i] University of Western Ontario, Electrical and Computer Engineering, London, Ontario, Canada N6A 5B9
[j] University of Maribor, Faculty of Energy Technology, Hocevarjev trg 1, 8270 Krsko, Maribor, Slovenia

ARTICLE INFO

Article history:
Received 15 June 2010
Received in revised form
11 July 2010
Accepted 18 July 2010
Available online 21 August 2010

Keywords:
Thermochemical hydrogen production
Copper–chlorine cycle

ABSTRACT

This paper presents an overview of the status of Canada's program on nuclear hydrogen production and the thermochemical copper–chlorine (Cu–Cl) cycle. Enabling technologies for the Cu–Cl cycle are being developed by a Canadian consortium, as part of the Generation IV International Forum (GIF) for hydrogen production with the next generation of nuclear reactors. Particular emphasis in this paper is given to hydrogen production with Canada's Super-Critical Water Reactor, SCWR. Recent advances towards an integrated lab-scale Cu–Cl cycle are discussed, including experimentation, modeling, simulation, advanced materials, thermochemistry, safety, reliability and economics. In addition, electrolysis during off-peak hours, and the processes of integrating hydrogen plants with Canada's nuclear plants are presented.

1. Introduction

Climate change and urban air quality continue to be significant issues today with well documented environmental and health impacts. Hydrogen is a potentially major solution to the problem of climate change, as well as addressing urban air pollution issues. But a key future challenge for hydrogen as a clean energy carrier is a sustainable, low-cost method of producing it in large capacities. Most of the world's hydrogen (about 97%) is currently derived from fossil fuels through some type of reforming process (such as steam–methane reforming; SMR). Nuclear hydrogen production is an emerging and promising alternative to SMR for carbon-free hydrogen production in the future. This paper presents an overview of Canada's program on nuclear hydrogen production and the thermochemical Cu–Cl cycle, specifically with

* Corresponding author.
E-mail address: greg.naterer@uoit.ca (G.F. Naterer).
0360-3199/$ – see front matter © 2010 Professor T. Nejat Veziroglu. Published by Elsevier Ltd. All rights reserved.
doi:10.1016/j.ijhydene.2010.07.087

recent advances in Canada since the time of an earlier review paper by Naterer et al. [1].

Hydrogen is used widely by petrochemical, agricultural (e.g., ammonia for fertilizers), manufacturing, food processing, electronics, plastics, metallurgical, aerospace and other industries. For example, in Alberta, Canada, the oil sands sector needs vast amounts of hydrogen to upgrade bitumen to synthetic crude oil and remove impurities. Hydrogen has recently made significant commercial penetration with fuel cells in the lift-truck market, as well as back-up power systems for cell phone communication towers. In the transportation sector, major auto-makers are investing significantly in fuel cell vehicles, and there are a number of demonstration projects ongoing. Hydrogen is becoming an increasingly important energy carrier. It can be stored and used to generate electricity, either onboard vehicles or stationary power systems [2].

The transportation sector contributes significantly to GHG emissions in Canada. A fuel cell vehicle (FCV) and battery electric vehicle (BEV) are the two main transportation technologies that can achieve a major reduction in GHG emissions. Despite the promising capabilities of hybrid, plug-in hybrid, and electric vehicles, some ongoing challenges associated with battery powered vehicles include: long battery recharge times, limited storage capacity, cold weather performance, and durability in real-world conditions, among others. As a result, hydrogen will continue to have an important role in light duty vehicle powertrains as a "range extender" fuel in plug-in hybrid vehicles, or eventually as standalone hydrogen fuel cell vehicles. The envisioned future hydrogen economy in the transportation sector will require significant increases to the world's current capacity to generate hydrogen, particularly in a clean, sustainable manner without relying on fossil fuels.

Thermochemical water decomposition is an emerging technology for large-scale production of hydrogen. Typically using two or more intermediate compounds, a sequence of chemical and physical processes split water into hydrogen and oxygen, without releasing any pollutants externally to the atmosphere. These intermediate compounds are recycled internally within a closed loop. Previous studies have identified over 200 possible thermochemical cycles [3,4]. However, very few have progressed beyond theoretical calculations to working experimental demonstrations that establish scientific and practical feasibility of the thermochemical processes.

The sulfur–iodine (S–I) and hybrid sulfur cycles are prominent cycles that have been developed extensively by several countries. These include the USA (General Atomics, Savannah River National Laboratory, among others), Japan (Japan Atomic Energy Agency, JAEA), France (Commissariat à l'Energie Atomique, CEA), Italy and others [5,6]. About 30 l/h of hydrogen production has been demonstrated by an S–I pilot facility at JAEA [5]. Canada, Korea (KAERI), China and South Africa also have active programs in nuclear hydrogen production. The following seven cycles (in addition to the S–I and hybrid sulfur cycles) were identified in a Nuclear Hydrogen Initiative [4] as the most promising cycles: copper–chlorine (Cu–Cl) [7], cerium–chlorine (Ce–Cl) [8], iron–chlorine (Fe–Cl) [8], vanadium–chlorine (V–Cl) [8], copper-sulfate (Cu-SO_4) [8] and hybrid chlorine [8]. Experimental work has been conducted for processes in these cycles to demonstrate their scientific feasibility. However, most of these cycles require heat at temperatures over 800 °C from very high temperature (Generation IV) reactors, which are not currently available and entail major design and material challenges. The Cu–Cl cycle has a significant advantage over these other cycles, due to lower temperature requirements around 530 °C and lower. As a result, it can be eventually linked with the Generation IV SCWR (Super-Critical Water Reactor) or ultra-super-critical thermal stations.

Advantages of the Cu–Cl cycle over others include lower operating temperatures, ability to utilize low-grade waste heat to improve energy efficiency, and potentially lower cost materials. Another significant advantage is a relatively low voltage required for the electrochemical step (thus low electricity input), which will be further explained in this paper. Other advantages include common chemical agents and reactions going to completion without side reactions, and lower demands on materials of construction. Solids handling between processes and corrosive working fluids present unique challenges, however this paper will outline recent advances made towards the development of corrosion resistant materials for these working fluids.

The University of Ontario Institute of Technology (UOIT), Atomic Energy of Canada Limited (AECL), Argonne National Laboratory (ANL) and other partner institutions are currently collaborating on the development of enabling technologies for the Cu–Cl cycle, through the Generation IV International Forum (GIF; [7]). This paper describes the status of these enabling technologies for the Cu–Cl cycle, as well as other nuclear hydrogen research and development programs in Canada, including electrolysis during off-peak hours for hydrogen usage by the transportation sector. Experimental work on the Cu–Cl cycle, modeling and simulation, thermochemistry, corrosion resistant materials, safety, reliability and linkage between nuclear and hydrogen plants, will be presented and discussed in this paper.

2. Thermochemical copper–chlorine (Cu–Cl) cycle

2.1. *Description of the Cu–Cl cycle*

The Cu–Cl cycle performs a sequence of reactions to achieve the overall splitting of water into hydrogen and oxygen. Using intermediate copper chloride compounds, the cycle decomposes water into hydrogen and oxygen, in a closed internal loop that recycles all chemicals on a continuous basis. Process steps in the Cu–Cl cycle and a schematic realization of the cycle are shown in Table 1 and Fig. 1, respectively.

There are three key variations of the Cu–Cl cycle: 5-step, 4-step and 3-step cycles. In the 5-step cycle, copper is produced electrolytically, moved to an exothermic thermochemical hydrogen reactor and then reacted with HCl gas to produce hydrogen gas and molten CuCl. The 4-step cycle combines these processes together to eliminate the intermediate production and handling of copper solids, through a CuCl/HCl electrolyzer that produces hydrogen electrolytically and aqueous Cu(II) chloride. Afterwards, the aqueous

Table 1 – Steps and chemical reactions in the Cu–Cl cycle.

Step	Reaction	Temp. range (°C)	Feed output[a]	
1	$2CuCl\ (aq) + 2HCl\ (aq) \rightarrow H_2\ (g) + 2CuCl_2\ (aq)$	<100 (electrolysis)	Feed	Aqueous CuCl and HCl + V + Q
			Output	$H_2 + CuCl_2$ (aq)
2	$CuCl_2\ (aq) \rightarrow CuCl_2\ (s)$	<100	Feed	Slurry containing HCl and $CuCl_2$ + Q
			Output	Granular $CuCl_2 + H_2O$/HCl vapors
3	$2CuCl_2\ (s) + H_2O\ (g) \rightarrow CuO{\times}CuCl_2\ (s) + 2HCl\ (g)$	400	Feed	Powder/granular $CuCl_2 + H_2O$ (g) + Q
			Output	Powder/granular $Cu_2OCl_2 + 2HCl$ (g)
4	$CuO \times CuCl_2(s) \rightarrow 2CuCl(l) + 1/2O_2\ (g)$	500	Feed	Powder/granular $Cu_2OCl_2(s)$ + Q
			Output	Molten CuCl salt + oxygen

a: Q = thermal energy, V = electrical energy.

product is dried to generate Cu(II) chloride particles; then fed to a hydrolysis reactor to produce copper oxychloride. The 3-step cycle further combines these processes by supplying aqueous Cu(II) chloride directly into the hydrolysis chamber, such as spraying the solution with co-flowing steam to produce the same copper oxychloride product. This paper will focus on the 4-step cycle (Table 1), since separation of the hydrolysis and drying processes can significantly improve the cycle's thermal efficiency.

The overall efficiency of the Cu–Cl cycle is potentially much higher than conventional water electrolysis via thermal power plants, since heat is used directly to produce hydrogen, rather than indirectly to first produce electricity, after which hydrogen is generated. A 42% efficiency (electricity) with the Generation IV reactor (SCWR; Super-Critical Water Reactor) leads to about 30% net efficiency by electrolysis for hydrogen production. In contrast, a 54% heat-to-hydrogen efficiency has been demonstrated from Aspen Plus simulations for the Cu–Cl cycle [9], although 43% is more realistic. This is a significant margin of superior overall conversion efficiency, with more than one-third improvement over electrolysis, excluding larger gains if "waste heat" is utilized in the Cu–Cl cycle.

2.2. *CuCl/HCl electrolysis for hydrogen production (step 1)*

This section presents the recent advances in Cu(I) chloride/HCl electrolysis for electrochemical production of hydrogen. Oxidation of Cu(I) chloride (CuCl) during an electrochemical reaction occurs in the presence of hydrochloric acid (HCl) to generate hydrogen. The Cu(I) ion is oxidized to Cu(II) at the anode, and the hydrogen ion is reduced at the cathode. While the majority of the Cu species present is expected to be anionic (which would not permeate through a cation exchange membrane), an appreciable concentration of cationic or neutral Cu species still exists and can permeate through the membrane and enter the cathode compartment where they are reduced to metallic copper.

The CuCl/HCl electrolysis cell is depicted to Fig. 2. It has been demonstrated by AECL that hydrogen can be produced at a current density of 0.1 A cm^{-2} for a cell voltage in the range of 0.6–0.7 V. A schematic of the electrolysis cell and copper crossover process is illustrated in Fig. 2. Metallic copper at the cathode acts as a poison, greatly reducing the activity of the Pt catalyst towards the hydrogen evolution reaction (HER). This could result in a catastrophic decrease in cell performance, so

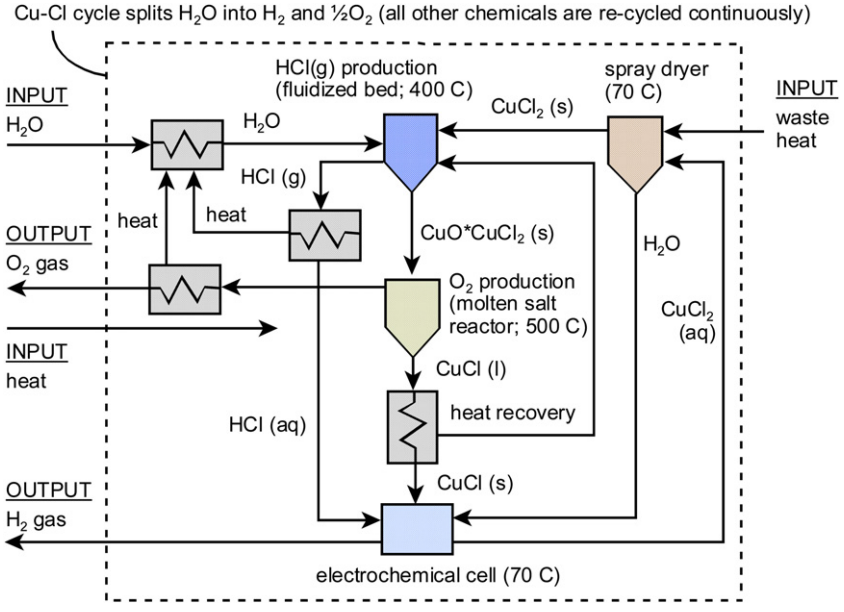

Fig. 1 – Schematic of the copper–chlorine (Cu–Cl) cycle.

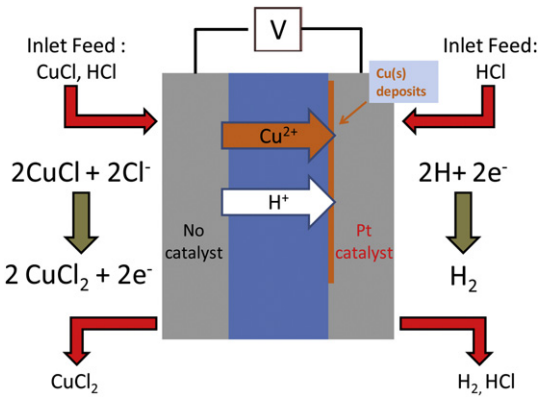

Fig. 2 – Schematic of CuCl/HCl electrolyzer and copper crossover.

active research is underway to eliminate any possible copper crossover.

The electrolysis efficiency of the process is defined as the voltage efficiency multiplied by current efficiency, where the voltage efficiency is the decomposition potential divided by the applied potential, and the current efficiency is the experimental H_2 production divided by the theoretical H_2 production. AECL has successfully demonstrated experimentally the production of hydrogen over a period of several days with a CuCl/HCl electrolyzer. Hydrogen is produced electrolytically at the cathode and Cu(I) chloride is oxidized to Cu(II) chloride at the anode. A schematic of the experimental layout is illustrated in Fig. 3.

The overall cell reaction can be expressed as

$$2CuCl + 2HCl \rightarrow 2CuCl_2 + H_2 \quad (1)$$

At the anode, several Cu(I) and Cu(II) chloride complexation species can form, via the following reactions:

$$Cu^{+}(aq) + nCl^{-} \leftrightarrow CuCl_n^{1-n} \quad (2)$$

$$Cu^{2+}(aq) + nCl^{-} \leftrightarrow CuCl_n^{2-n} \quad (3)$$

In chloride media, Cu(I) can exist as several different anionic species (e.g.$CuCl_2^-$, $CuCl_3^{2-}$). The relative ratios of each species are dependent on the concentration of chloride ions [10]. Regardless of the exact species present, the anodic reaction proceeds by the electro-oxidation of Cu(I) species into Cu (II) species.

The reversible cell potential for this reaction is −1.23 V. This implies that the free energy change for the electrochemical reaction is positive, so in order for it to proceed, energy must be added to the system. Recent studies have shown that the rate of the CuCl/HCl electrolysis reaction increases with temperature and CuCl concentration. A variety of electrode materials have been tested and hydrogen production was consistently observed at potentials as low as 0.5 V. However, approximately 0.65 V was typically required to achieve good current density. Promising results have successfully demonstrated that the reaction is feasible at low potentials and with relatively inexpensive electrode materials [11].

A membrane is required to separate the anode side of the electrolysis cell from the cathode side. A major issue under investigation for the cation exchange membrane is copper species crossing the membrane from the anode side to the cathode side of the cell. At the anode side of the electrolysis cell, Cu(I) chloride is oxidized to Cu(II) chloride according to the following equation: $CuCl_4^{3-}$ (or $CuCl_3^{2-}$ if the concentration of chloride is lower than 5 M) → $CuCl_2$ (plus other Cu(II)

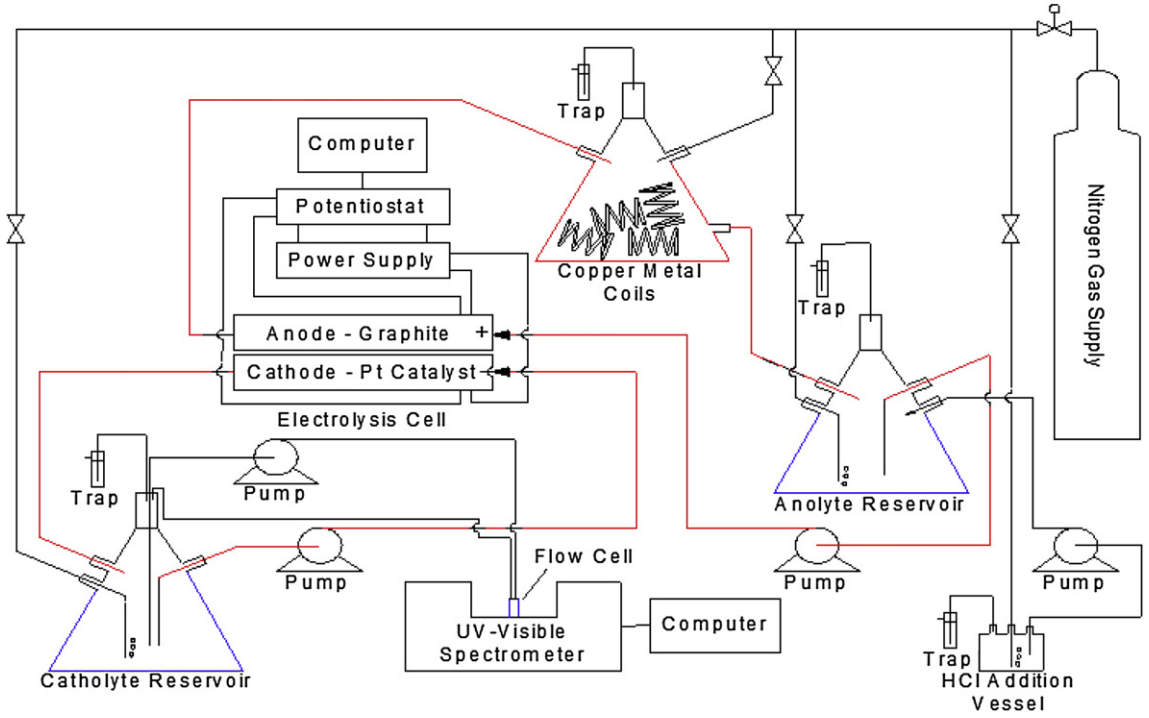

Fig. 3 – Schematic of single-cell process flow configuration.

chloride species if the concentration of chloride is greater than 5 M) + $2Cl^- + e^-$. This reaction could occur if the free chloride ion concentration is above 4 M. In recent experiments, the anolyte is a solution of CuCl dissolved in 0.5–2 M HCl. The Cu(I) oxidation reaction does not require a catalyst. The anode is a catalyst-free fuel cell graphite separator plate material.

This reaction at the cathode ($2H^+ + 2e^- \rightarrow H_2$) describes the reduction of protons to form hydrogen gas. The cathode is a fuel cell graphite separator plate coated with a Pt electrocatalyst. Fig. 4 illustrates the measured cell potential over approximately 3 days of continuous hydrogen production. In the experiments, the catholyte and anolyte HCl concentrations are 6 and 10 M, respectively. The CuCl concentration in the anolyte is 1.0 M. When 10 M HCl is used instead of 6 M HCl, the performance of the cell improves significantly. The catholyte passed through the cathode compartment a single time, while the anolyte was recycled. The measured oscillations in Fig. 4 reflect temperature variations in the lab, overnight vs. daytime. Over a 72 h period, the cell potential changed by 0.016 V.

Fig. 5 shows that increasing the HCl concentration decreases the amount of copper species present in the catholyte. Each data set was fitted to a second order polynomial in Fig. 5. The data suggests that copper chloride speciation in the anolyte depends on the HCl concentration. The experiments indicated that relatively stable cell potentials can be measured when the catholyte solution is not recycled, but passes through the cathode compartment of the electrolysis cell a single time. The catholyte copper species concentration decreases as the HCl concentration increases. It was found that the CuCl/HCl electrolysis reaction should be performed with an HCl concentration of at least 11 M, so copper metal deposition does not occur at a current density of 0.1 A/cm^2. The catholyte copper species concentration increases as the CuCl concentration increases. Thus, low CuCl concentrations are preferred. The preferred anolyte concentration is 0.5 M CuCl in 11 M HCl, while the preferred catholyte concentration is 11 M HCl.

Additional laboratory scale CuCl/HCl electrolyzer experiments have also been performed at Pennsylvania State University [11] to determine the electrolysis efficiency. Electrolysis with a Nafion-based proton conductive membrane

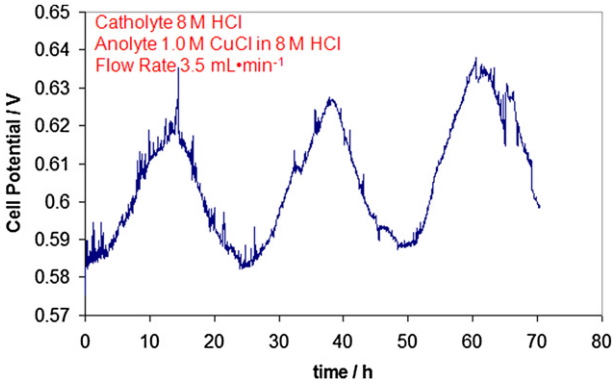

Fig. 4 – Varying cell potential over a period of about 3 days of hydrogen production.

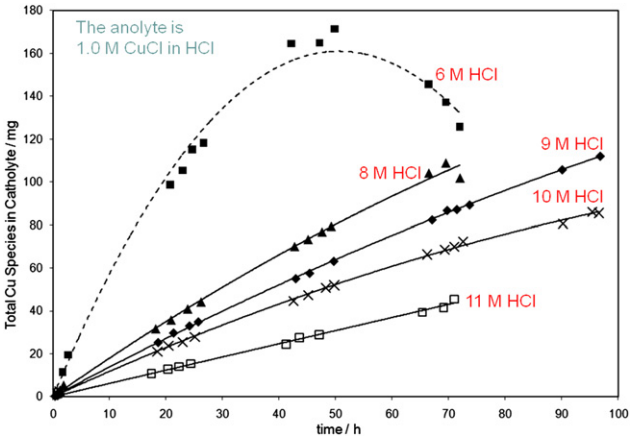

Fig. 5 – Effects of HCl concentration on total catholyte copper.

was shown to be a highly efficient process. The measured current efficiency was around 98% and the voltage efficiency was up to 80% for usable current densities. In Fig. 6, the filled circles depict the best obtained results with a HYDRion115 MEA. The other curves refer to a number of experimental conditions tested with lower performance. The experimental results in Fig. 6 by Lvov et al. [11] at Pennsylvania State University were obtained independently and with different membranes than AECL results reported in Figs. 4 and 5. The catholyte is 0.2 mol kg^{-1} CuCl in 2 mol kg^{-1} HCl (aq), the anolyte is H_2O, the catholyte flow rate is 68 cm^3 min^{-1}, and the temperature is 30 °C. Ongoing research aims to optimize the MEA preparation to achieve a target performance of 0.5 A/cm^2 at 0.7 V, and completely eliminate the Cu permeation through the membrane.

2.3. *Drying of aqueous Cu(II) chloride (step 2)*

Step 2 of the Cu–Cl cycle is the drying step as expressed by: $2CuCl_2$ (aq) → $2CuCl_2$ (s) (see Table 1). Aqueous $CuCl_2$ exiting from the previous electrolysis cell is dried to produce solid

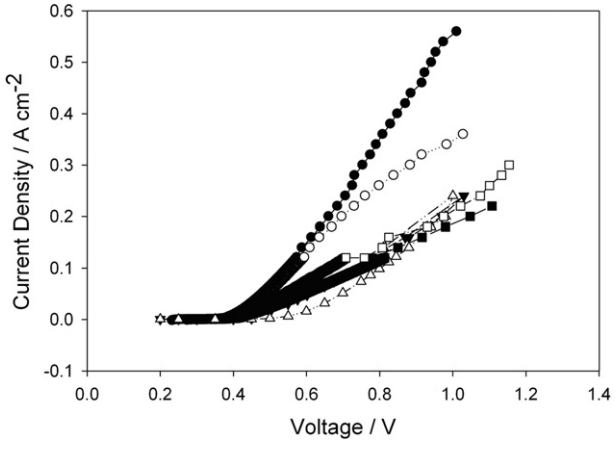

Fig. 6 – Measured polarization curves for CuCl/HCl electrolysis.

$CuCl_2$ (s), which is required for a subsequent hydrolysis step that produces copper oxychloride ($CuO \times CuCl_2$) and HCl gas. The drying process is an energy-intensive step within the Cu–Cl cycle. Although the amount of heat required for the drying step is much higher than other steps in the cycle, it occurs at a lower temperature (lower quality) and therefore with heat that is more readily available. Within the drying step, the energy requirement increases from 1 to 5 times higher for slurry feed to solution, respectively, depending on the $CuCl_2$ concentration. The required heat can be obtained from low-grade "waste" heat to improve the cycle efficiency. Spray drying is an efficient method of water removal due to the relatively large surface area available for heat and mass transfer, provided the liquid atomizes into sufficiently small droplets (on the order of a few hundred microns).

Experimental spray drying studies have been performed to produce solid Cu(II) chloride particles from an aqueous $CuCl_2$ solution. Spray drying is a well established industrial process that allows powder characteristics and properties to be controlled and maintained nearly constant throughout a drying operation. The experimental apparatus for drying of aqueous Cu(II) chloride and sample dried $CuCl_2$ particles are illustrated in Figs. 7 and 8, respectively. The following spray dryer conditions were used in the experiments: inlet air temperature = 200 °C, outlet air temperature = 112 °C, atomizing gas pressure = 2 bar, inlet gas pressure = 30 mbar, total mass of product = 183 g, and density of product = 0.7 g/cm^3. The bulk density of the product is 0.59 g/cm^3 and the tapped density is 0.7 g/cm^3. Current research is performing experimental studies at successively lower inlet air temperatures, in order to eventually utilize waste heat from thermal power plants or other industrial sources for the spray drying heat requirements.

Numerical studies [12–14] were also conducted to analyse the process of spray drying of aqueous Cu(II) chloride droplets. Fig. 9 illustrates that the drying time depends on the inlet air humidity, velocity, temperature and particle size. At a humidity of 0.0025 kg water/kg dry air, the drying time is less than 6 s for droplet sizes of 200 μm at 35 °C. At a humidity of 0.01 kg water/kg dry air, the drying time is less than 6 s for droplet sizes of 100 μm at 35 °C, and droplet sizes of 150 μm at air velocities above 3 m/s. The results indicate that evaporative drying is possible down to low temperatures as low as 35 °C, although such low temperatures may limit the product throughput rate.

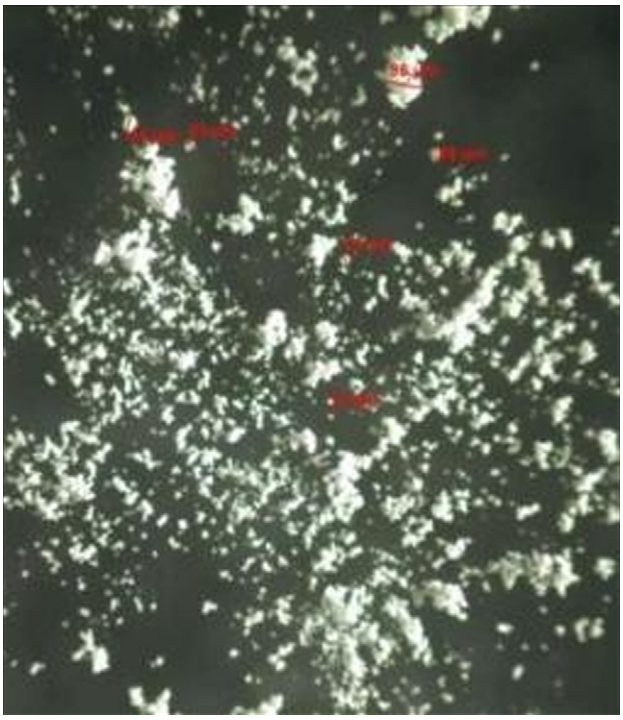

Fig. 8 – Sample dried Cu(II) chloride particles.

2.4. *Hydrolysis reaction (step 3)*

The following hydrolysis reaction occurs within the Cu–Cl cycle (see Table 1): $H_2O(g) + 2CuCl_2(s) \rightarrow Cu_2OCl_2(s) + 2HCl(g)$. The reaction is an endothermic non-catalytic gas–solid reaction that operates between 350 and 400 °C. The solid feed to the hydrolysis reaction is Cu(II) chloride, from the dried $CuCl_2$ product of step 2. Aqueous Cu(II) chloride is dried in step 2 to produce $CuCl_2$ particles, which are then moved to the hydrolysis unit and reacted with superheated steam to produce copper oxychloride solid and hydrochloric gas. This section describes recent developments in both experimental and numerical studies of transport phenomena associated with the non-catalytic gas–solid reaction of hydrolysis of Cu(II) chloride.

Lewis et al. [9] have demonstrated experimentally the scientific practicality of the hydrolysis reaction to produce HCl

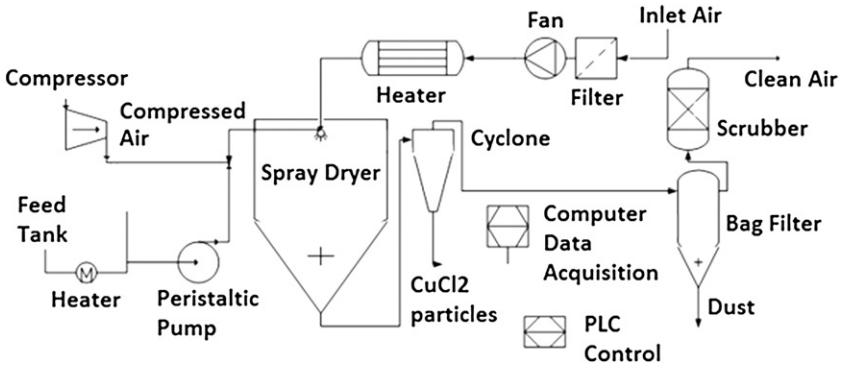

Fig. 7 – Experimental facility for Cu(II) chloride spray drying.

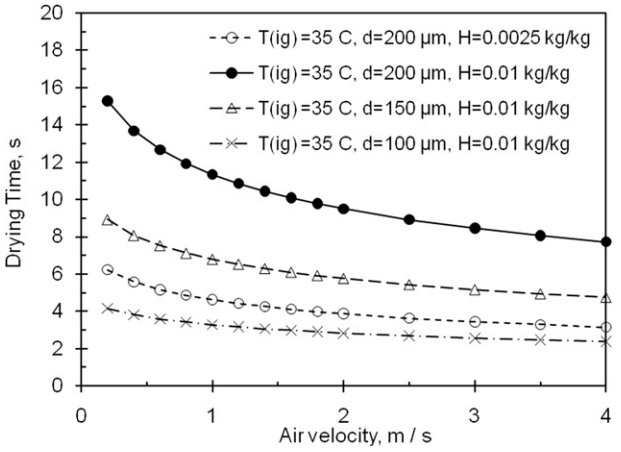

Fig. 9 – Variation of drying time with air velocity, humidity and droplet size.

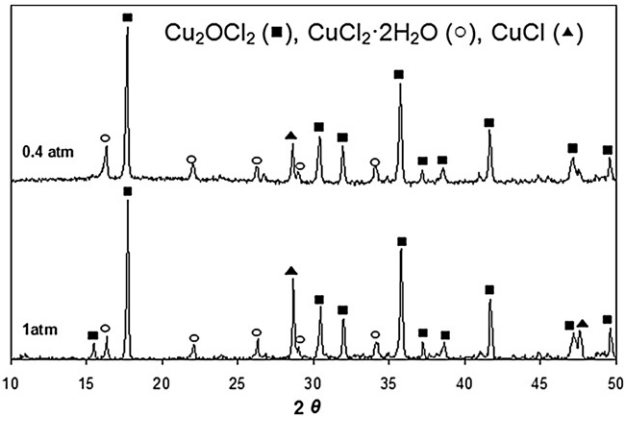

Fig. 11 – XRD patterns for products at 0.4 and 1 bar (steam to $CuCl_2$ ratio = 11.

gas and solid copper oxychloride. Experimental results and simulations showed a large excess of water was needed for complete conversion (up to 98%) of $CuCl_2$. Byproducts other than Cu_2OCl_2 may appear, i.e., CuCl and CuOHCl, although ongoing research is investigating how and why these byproducts appear. For an efficient and low capital cost process, it is important to reduce the water consumption. Aspen Plus simulations predict that 100% yield can be obtained with steam to a $CuCl_2$ molar ratio of 17 at 370 °C [9].

In recent experiments, a range of steam to $CuCl_2$ molar ratios was used in the hydrolysis spray reactor at the Argonne National Laboratory. It was found that water requirements could be reduced by using sub-atmospheric pressures. For complete conversion, Aspen Plus sensitivity studies indicate a steam to Cu(II) chloride molar ratio of about 18 for 1 bar, and about 12 for 0.5 bar (see Fig. 10). Adding an aspirator to the hydrolysis reactor allows operation of the reactor at reduced pressures: 0.4 and 0.7 bar tests were conducted. The reactor was flushed with more humid inert gas in the experiments. The steam demand and CuCl formation were reduced. Fig. 11 illustrates the XRD patterns for various Cu–Cl compounds. It was observed that all experiments at reduced pressure had lower CuCl content.

Unlike a spray reactor (ultrasonic nozzle) used by the Argonne National Laboratory for the hydrolysis reaction, UOIT experiments have separated the drying and reaction processes, thereby using separate steps 2 (drying) and 3 (gas–solid reaction in a fluidized bed for hydrolysis). At UOIT, high temperature fluidized bed experiments with actual Cu–Cl compounds are being investigated, as well as low temperature experiments with simulated working fluids (air and spherical beads) to examine fluid dynamics and heat transfer phenomena in the fluidized bed. Fig. 12 illustrates the layout of the high temperature experiments. In Fig. 13, measured results of pressure drop in the low temperature experiments are shown, which are useful to improve the optimal packing density of particles and solid conversion rates.

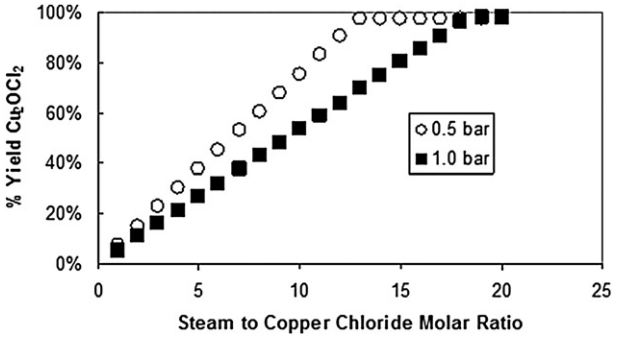

Fig. 10 – Percentage yields of copper oxychloride.

The experimental unit was designed similar to the high temperature hydrolysis reactor, both geometrically and dynamically, by matching the Archimedes number, Froude number, density ratio, particle to column diameter and particle size distribution. The solid to gas density ratio is matched for accurate scaling of the hydrodynamics in a bubbling or turbulent bed. The fluidized bed unit is made of plexiglass with a 0.1 m diameter and 0.6 m test section. The gas distributor consists of seven nozzles equally and symmetrically spaced over the bottom plate. Instantaneous pressure measurements are taken with Omega, PX140 pressure transducers, two differential (15 psi) and one absolute (30 psi). For each experiment, 10,000 data points were collected at a frequency of 100 Hz. The measured data was processed by means of statistical algorithms to obtain the standard deviations and average pressure drops. The experimental data indicated the importance of the pressure drop on the fluidization quality at high temperatures. Variations of particle properties at high temperatures reduce the fluidization quality. The measurements of pressure fluctuations provided useful data for monitoring the behavior of the high temperature hydrolysis reactor.

Additional numerical and experimental studies have been performed to investigate the transport phenomena associated with the gas–solid reaction of particles in the fluidized bed during hydrolysis of Cu(II) chloride ([15–18]; see Fig. 14). The conversion of solids depends on the rate of reaction and residence time of a particle. A shrinking-core model (SCM) has

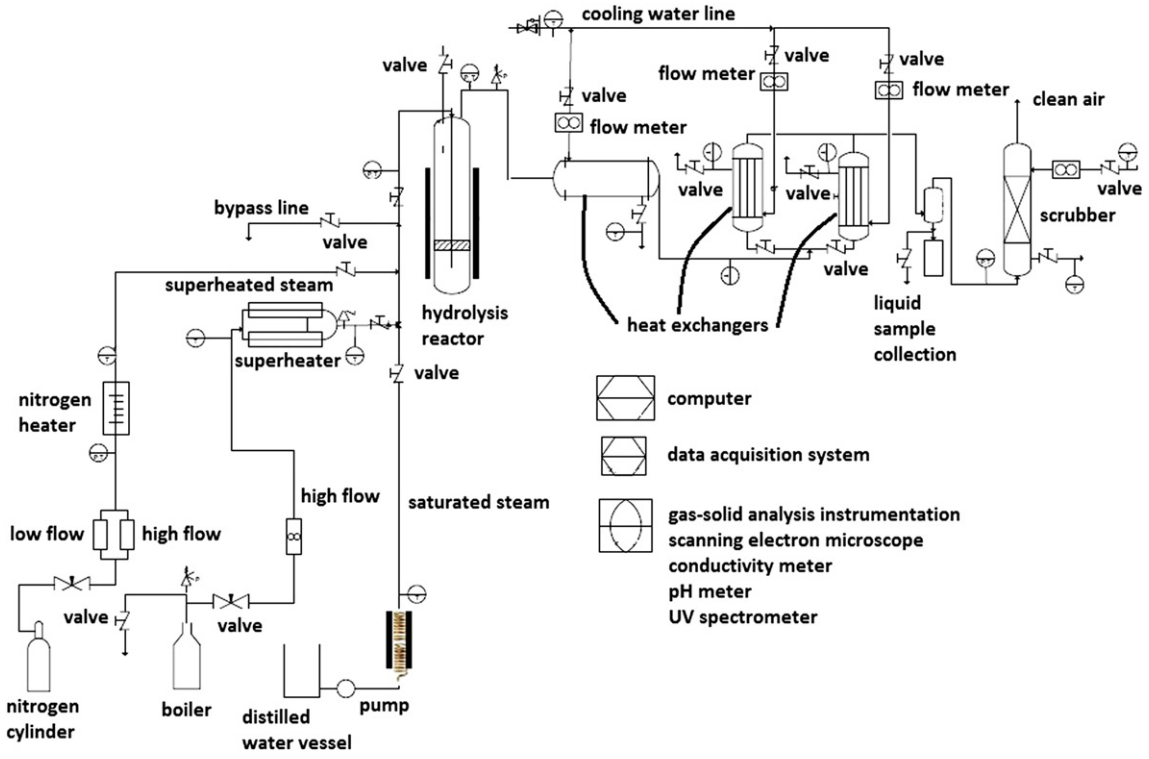

Fig. 12 – Schematic of hydrolysis experiments with a fluidized bed reactor.

been developed to estimate the reaction rate of the gas–solid reaction. When the diffusion of gaseous reactant into a particle is much faster than the chemical reaction, the solid reactant is consumed nearly uniformly throughout the particle (see Fig. 14a). In this situation, a uniform-reaction model can be used. On the other hand, when the diffusion of gaseous reactant is much slower and it restricts the reaction zone to a thin layer that advances from the outer surface into the particle (Fig. 14b), then the shrinking-core model is adopted. The predicted variation of solid conversion time with vapor fraction in the gas is illustrated in Fig. 15. Close agreement is achieved with measured data of solid conversion for uniformly sized particles of 200 μm diameter in plug flow of solids. As the mole fraction of steam in the gas increases, the time of solid conversion decreases.

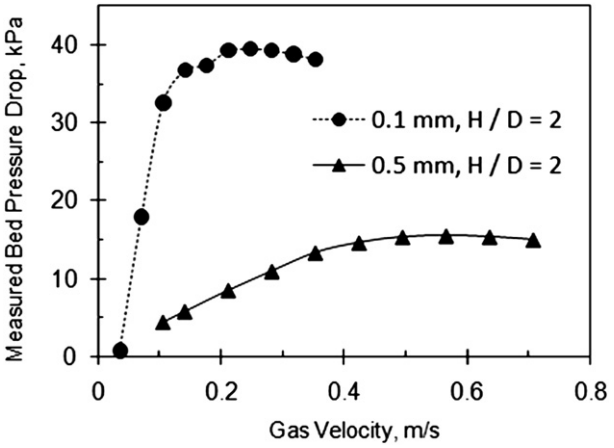

Fig. 13 – Measured pressure drop in the fluidized bed.

2.5. *Copper oxychloride decomposition (step 4)*

The oxygen production step (step 4; see Table 1) receives solid feed of copper oxychloride (Cu_2OCl_2) and produces O_2 gas and molten Cu(I) chloride. The decomposition reaction is given by Cu_2OCl_2 (s) = 2CuCl (molten) + $0.5O_2$ (gas) at 530 °C. Copper oxychloride particles decompose into molten salt and oxygen gas bubbles. The reactant particles absorb decomposition heat from the surrounding molten bath. Gas species leaving the oxygen reactor include oxygen gas and potentially impurities of products from side reactions, such as CuCl vapor, chlorine gas, HCl gas (trace amount) and H_2O vapor (trace amount). The substances exiting the reactor are molten CuCl, potentially unreacted solid $CuCl_2$ from the upstream hydrolysis reaction, due to the incomplete decomposition of $CuCl_2$, as well as reactant particles entrained by the flow of molten CuCl (Fig. 16).

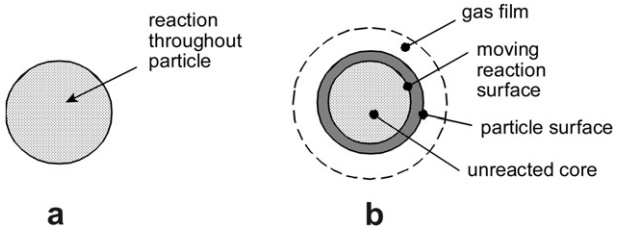

Fig. 14 – Schematic of (a) particle conversion and (b) particle shrinkage with an ash layer and gas film.

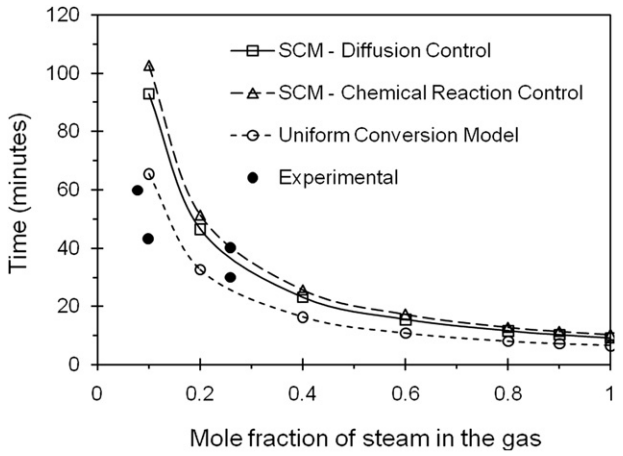

Fig. 15 – Comparison of solid conversion time with experimental data.

Serban et al. [19] have demonstrated experimentally the scientific practicality of the oxygen production reaction at a small test-tube scale. Recent advances have demonstrated experimentally the processes in a larger engineering scale reactor, with flow capacities of 2 kg/day of oxygen production, by decomposing about 21 kg/day of solid Cu_2OCl_2 feed that enters the reactor. A number of experimental and operational issues with the unit reactor are currently being investigated, such as aggregation into solid blocks of Cu_2OCl_2 when conveying and feeding solid particles. The aggregation may choke or clog the feeder and cause sudden spouting of particles. Also, embedded particles of $CuCl_2$ from the upstream hydrolysis reactor in Cu_2OCl_2 may lead to undesirable products and side reactions, such as $CuCl_2$ decomposing to CuCl and Cl_2 gas. If particles enter the reactor at a temperature lower than 430 °C, a challenge arises with the presence of bubbles in the molten salt. Some CuCl vapor might condense and molten CuCl can solidify around the Cu_2OCl_2 particles. If an aggregation develops with particles, molten salt and bubbles, the contact area between a reactant particle and heating medium (molten CuCl) will decrease and the aggregations float along the surface of the molten salt. This deters the decomposition of reactant particles and potentially leads to choking of the reactor (a major safety concern). These issues and others are currently under investigation for the copper oxychloride decomposition experiments.

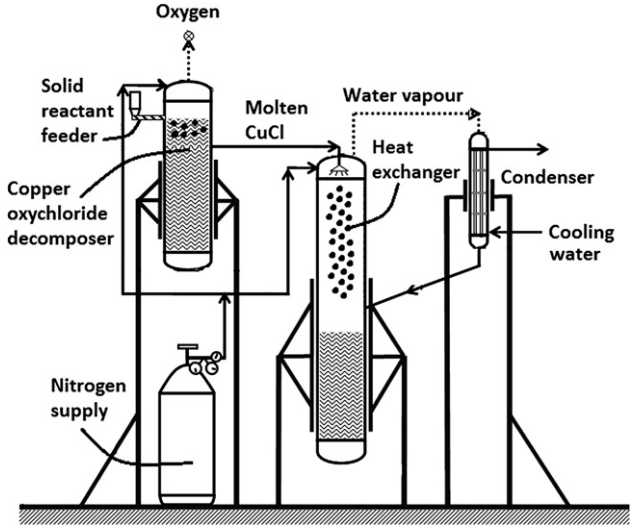

Fig. 16 – Schematic of oxygen decomposition reactor.

Additional studies have also been performed to effectively recover heat from molten CuCl exiting the copper oxychloride decomposer. A configuration with convective heat transfer between molten CuCl droplets and air in a counter-current spray flow heat exchanger has been developed (see Fig. 17). Recovering heat from molten CuCl is challenging due to the phase transformations of molten CuCl, as it cools from liquid to two different solid states. A predictive model of heat transfer and CuCl droplet flow has been developed and solved numerically [20]. The results indicated that full heat recovery can be achieved with a heat exchanger diameter of 0.13 m, and heights of 0.6 and 0.8 m, for a 1 and 0.5 mm droplet diameter, respectively. Other configurations of heat recovery from molten CuCl have been reported by Ghandehariun et al. [21].

Fig. 18 shows the variation of the heat transfer rate for droplets with 1 and 0.5 mm diameters throughout the height of the heat exchanger. The larger droplet diameter has a higher heat transfer rate, due to the larger surface area. The heat transfer rate increases initially at the bottom of the heat exchanger, because of the large temperature difference between both streams. Then it reaches a maximum when the second phase transformation ends, after which it decreases, due to the lower temperature difference between both fluids in the phase transformation process. When the second sensible heat transfer process is completed, the heat transfer rate starts increasing again. This does not take long because the first phase transformation differs with the second phase change process by 11°.

3. System modeling for cycle modifications and enhancements

3.1. *Aspen Plus simulations*

Aspen Plus simulations of the Cu–Cl cycle have been performed at the Argonne National Laboratory ([22]; see Fig. 19) and UOIT [23]. In Fig. 19, the cycle is based on four unit operations, all commercially practiced in industry: hydrolysis and oxychloride decomposition reactors, direct heat exchanger, electrolyzer and crystallizer. The simulations indicated that the steam requirement was reduced by operating the hydrolysis reactor at a partial vacuum, obtained by an ejector (similar to an aspirator). Spent anolyte can be processed to provide $CuCl_2$ slurry for the hydrolysis feed with minimal costs in energy and capital by crystallization. The cell voltage used for the electrolyzer was 0.7 V with a current density of 500 mA/cm^2. The electrolyzer operates at temperatures above 80 C and 24 bar. The flowsheet uses a reduced pressure in the hydrolysis reactor, 0.25 bar, in the simulations.

The amount of steam impacts the hydrogen production costs significantly. Handling and condensing the effluent steam from the hydrolysis reactor is being investigated, in

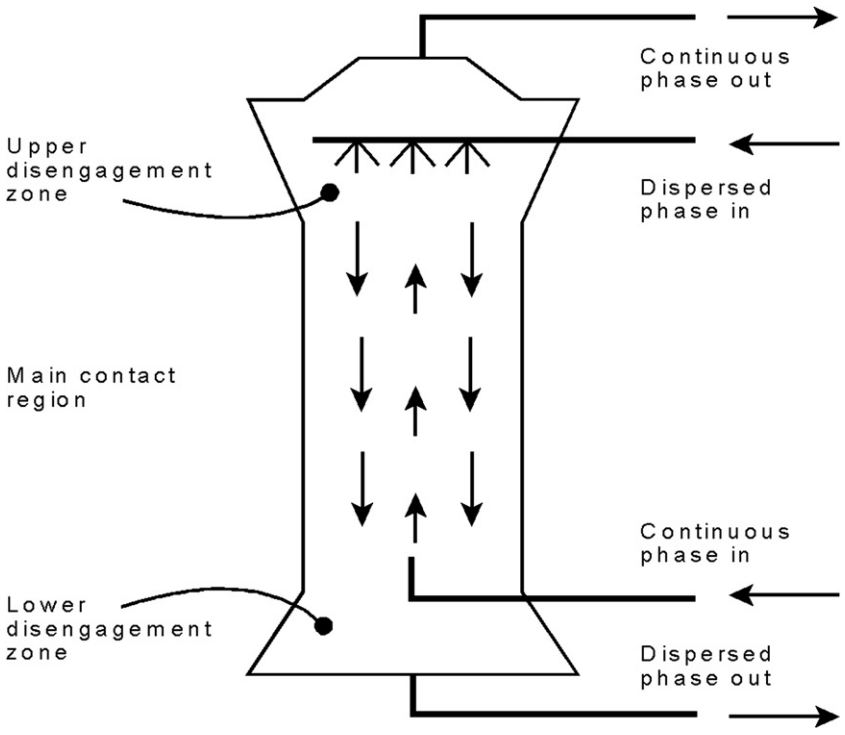

Fig. 17 – Schematic of molten CuCl heat recovery and problem parameters.

order to reduce the steam consumption requirements. It is inefficient to condense and then re-vaporize the water. Partial condensation of the effluent is another alternative under investigation. Modifications of the Cu–Cl cycle to reduce the steam requirements have been reported by Wang et al. [24].

Crystallization was studied as an alternative separation method to remove $CuCl_2$ from spent aqueous anolyte containing $CuCl_2$, CuCl and HCl. The CuCl cannot be all converted to $CuCl_2$ electrolytically. Only about 75% of the CuCl will be oxidized, and precipitation results in HCl and CuCl entrainment. Also, crystallization is energy intensive. The spent anolyte is cooled to 55 °C to effect separation. The $CuCl_2$ slurry must be reheated to the hydrolysis reactor temperature, which requires a large heat input. The spent anolyte may be relatively dilute. A more efficient method is needed to handle the spent anolyte consisting of $CuCl_2$, CuCl and HCl. A new experimental concept under investigation by ANL uses waste oxygen and eliminates temperature cycling as follows: $2CuCl + 0.5O_2 + 2HCl = 2CuCl_2 + H_2O$. Other potential methods under investigation are membrane distillation (using waste heat) and water removal by spray drying (discussed in Section 2.3). Several variations of cycle modifications have been examined [25], for which optimization techniques are also being developed to allow designers to identify optimal system parameters and operating conditions that minimize costs of hydrogen production.

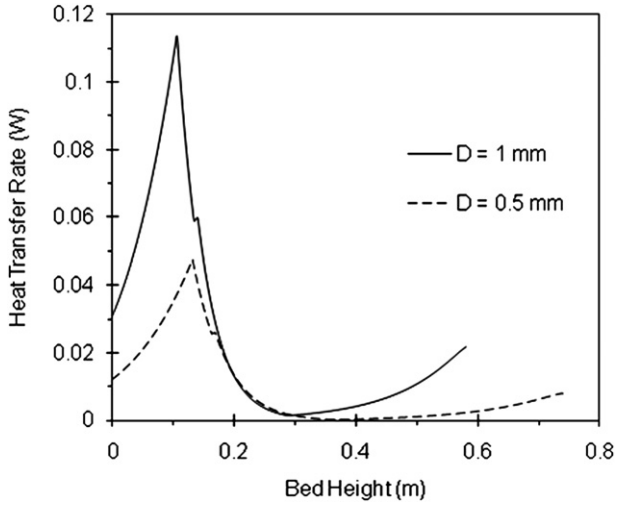

Fig. 18 – Heat transfer between molten CuCl droplets and co-flowing gas stream.

3.2. *Exergo-economic modeling*

Exergo-economic analysis using exergy-cost–energy-mass (EXCEM) provides a quantitative relationship between capital costs and thermodynamic losses. Recent EXCEM studies at UOIT have examined these features of the Cu–Cl cycle, to examine costs for improving the economic viability of the cycle [26–32]. The overall energy and exergy efficiencies of the entire cycle were reported for several different cases, i.e., varying reaction temperatures, environment temperatures, pressures, chemical compositions, etc. In addition, the recent studies compared the Cu–Cl cycle costs against other energy options such as fossil fuels (coal and natural gas) and renewable energies (solar, wind, hydro, geothermal and biomass). Several options were examined, including nuclear

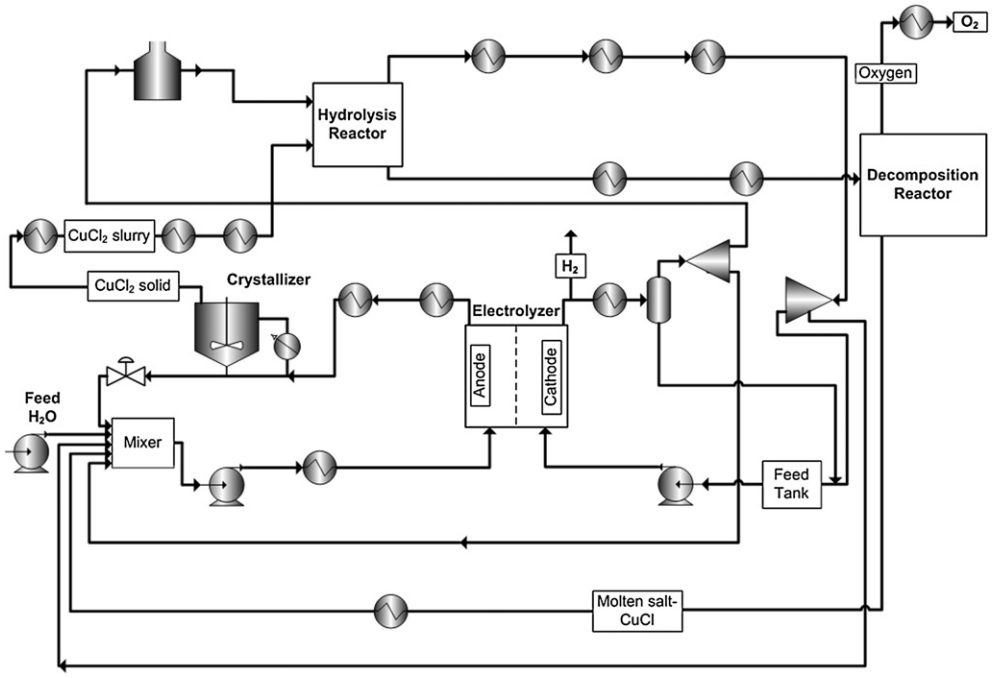

Fig. 19 – Simplified process flow diagram for one Aspen Plus simulation.

with/without other renewable energy systems, usage of a Cu–Cl cycle in off-peak hours, and integrated systems where thermochemical generated hydrogen is stored and then converted back to electricity when needed, via fuel cells. A thermodynamic analysis using energy and exergy, as well as several parametric studies, were conducted for various configurations of coupled systems to assess and compare their efficiencies.

The overall energy efficiency of the coupled system, $\eta_{overall}$, represents both the efficiency of the energy source and the hydrogen production technology, namely the Cu–Cl cycle. The overall efficiency can be expressed as

$$\eta_{overall} = \eta_{energy\ source} \times \eta_{Cu-Cl} \tag{4}$$

The efficiency of the Cu–Cl cycle is expressed as

$$\eta_{Cu-Cl} = \frac{HHV_{H_2}}{E_{in,\ Total}} = \frac{HHV_{H_2}}{(Q+W)_{in}} \tag{5}$$

where HHV, E, Q and W represent the higher heating value, energy, heat and electrical work (electricity), respectively. The HHV of 286 kJ/mol (used in these studies) is the energy gained from burning hydrogen in oxygen at ambient conditions, with initial and final conditions at the same 1 bar and 25 °C. The LHV of 236 kJ/mol assumes water is produced at 150 °C, from an initial state of 25 °C, and the energy of vaporization is not recuperated.

The cost of hydrogen production consists of (a) the energy cost, (b) raw material cost, and (c) capital costs (including operational and maintenance costs). The only raw input material to the Cu–Cl cycle is water, assumed to be no cost, so the cost of produced hydrogen becomes

$$\dot{C}_{H_2} = \dot{C}_{energy} + \dot{Z} \tag{6}$$

where $\dot{C}$ denotes the cost rate of the respective stream and $\dot{Z}$ the cost rate associated with owning and operating the cycle. The cost rates are expressed in units such as ($/h) or ($/kg H_2) for example. Equation (6) states that the total cost of the exiting streams (hydrogen) equals the total expenditure to obtain them, i.e., cost of the entering streams plus the capital and other costs. Since the entering streams to the Cu–Cl cycle are heat and electricity, Eq. (6) can be written as

$$\dot{C}_{H_2} = \dot{C}_{Heat} + \dot{C}_{Electricity} + \dot{Z} \tag{7}$$

In these studies, the cost of oxygen was not included, however oxygen is a useful byproduct that can be sold and used in industrial processes. In this case, the price of

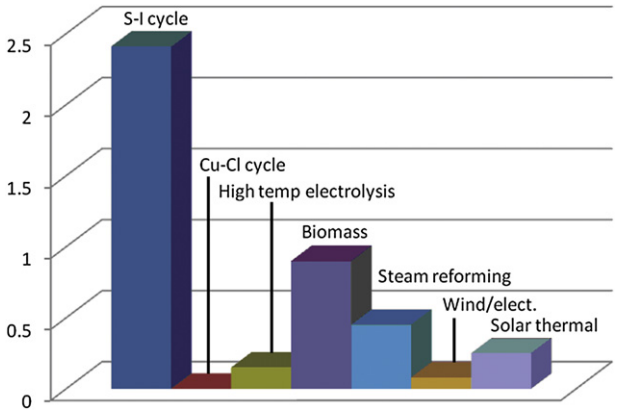

Fig. 20 – Acidification potential of hydrogen production methods.

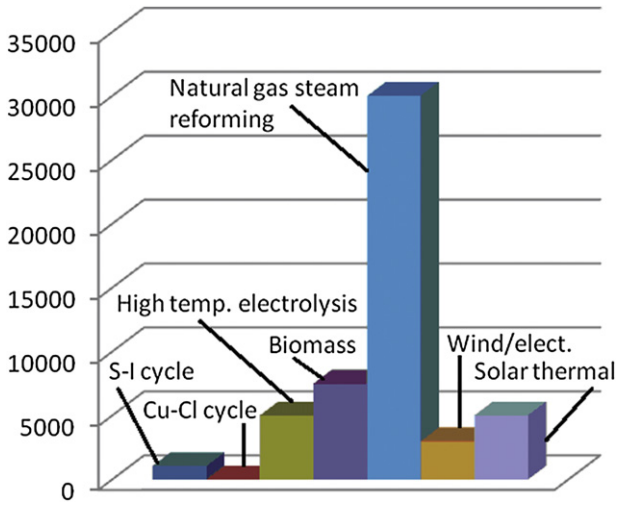

Fig. 21 – Eco-indicator values for hydrogen production methods.

produced oxygen should be reduced from the cost of produced hydrogen. In the past studies by Orhan et al. [26–32], the costs associated with various operations in the Cu–Cl cycle were examined. It was found that the capital cost is high for relatively small scale production capacity, and inversely proportional to the plant's capacity. For small scale production capacity (less than 50 tons H_2/day), capital costs of the cycle account for a major portion of the overall cost, in comparison to storage and distribution costs. In contrast, for large-scale production (>50 tons/day), storage becomes a major cost portion.

3.3. *Life cycle assessment*

In addition, system analysis for a life cycle assessment (LCA) was reported ([33]; see Figs. 20 and 21). It analyzed the environmental emissions and impacts, based on categories shown in Table 2. Emissions from the overall system are the sum of outputs from the nuclear plant and thermochemical hydrogen plant. The life cycle assessment of hydrogen production with the thermochemical Cu–Cl cycle was compared against other hydrogen production methods. For the environmental impact of hydrogen production by the thermochemical S–I cycle, the study of Solli et al. [34] was used. Utgikar et al. [35] investigated the environmental effect of high temperature electrolysis for hydrogen production via nuclear energy and compared it against other methods.

Fig. 20 shows the acidification potential of various methods. The results indicated that the Cu–Cl cycle has the lowest magnitude. To find the overall environmental impact, the Eco-indicator 95 method was applied. In order to perform the analysis, the acidification potential is multiplied by 10 and then GWP is multiplied by 2.5 [36]. Afterwards, these values are added. Fig. 21 shows the overall environmental impact, again showing the Cu–Cl cycle with the lowest environmental impact.

3.4. *Utilizing waste heat and heat pumps*

A unique advantage of the Cu–Cl cycle is its ability to utilize low-grade "waste heat" from power plants or other sources to aid hydrogen production, rather than rejecting that heat to the environment (such as a nearby lake). This could significantly improve the economics of hydrogen production, as well as potentially the generation of electricity. For example, a nuclear plant's efficiency usually refers to electricity output alone, but the "efficiency" would be higher if nuclear energy contributed to production of another valuable energy carrier, hydrogen, from the same nuclear source. The Cu–Cl cycle's efficiency implies that the heat supply comes at some "cost". But if low-grade waste heat is utilized as a heat source at minimal or no cost, then the economics of hydrogen production is improved and advantageous over other high temperature thermochemical cycles that cannot use such low-grade heat.

Drying of aqueous Cu(II) chloride (step 2; Table 1) is an energy-intensive process that requires heat at a relatively low temperature, below 100 °C. Waste heat at 75 °C from the moderator vessel of CANDU nuclear reactors could be transferred by fluid through a pipeline over some distance to a nearby thermochemical hydrogen plant. Flow through a liquid–gas heat exchanger would then transfer this waste

Table 2 – Environmental impact categories and definitions.

Environmental Impact Category	Definition
Abiotic resource depletion potential (ADP) (g extracted element)	Abiotic depletion involves the extraction of Non-renewable raw materials
Global warming potential (GWP) (g CO_2-eq)	Amount of CO_2 in the earth's atmosphere
Ozone depletion potential (ODP) (g CFC-eq)	Depletion of ozone layer leads to an increase in the ultraviolet radiation reaching the earth's surface
Eutrophication potential (EP) (kg phosphate-eq)	Over-fertilisation or nutrition enrichment at a certain location
Acidification potential (AP) (g SO_2-eq)	Acid depletion on soil and into water may lead to changes in the degree of acidity
Photochemical ozone creation potential (POCP) (kg ethene-eq)	Due to volatile organic compounds in the atmosphere
Radioactive radiation (RAD) (disability-adjusted life years, DALY)	Emission and propagation of energy in the form of rays or waves

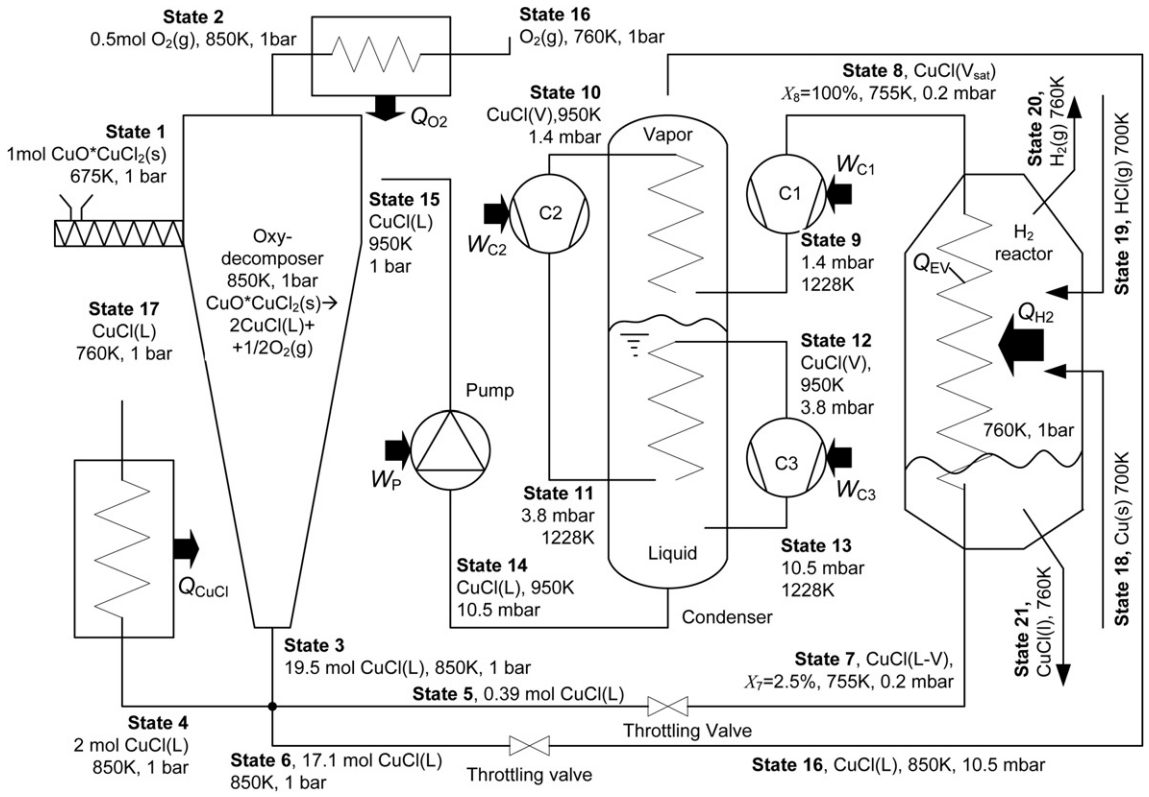

Fig. 22 – Schematic of CuCl vapor compression heat pump integrated with Cu–Cl cycle.

heat to a gas stream, which would be used as a drying medium in a spray dryer to produce $CuCl_2$(s) in the Cu–Cl cycle. Currently a shell and tube heat exchanger is used in CANDU nuclear plants for heat rejection from the moderator vessel, with heavy water on the tube side and lake water on the shell side. To utilize waste heat from the tube side, an intermediate heat exchanger is needed, in order to ensure no tritium transport from the heavy to light water side into the hydrogen plant [37]. Additional safety considerations are needed to handle linkage between nuclear and hydrogen

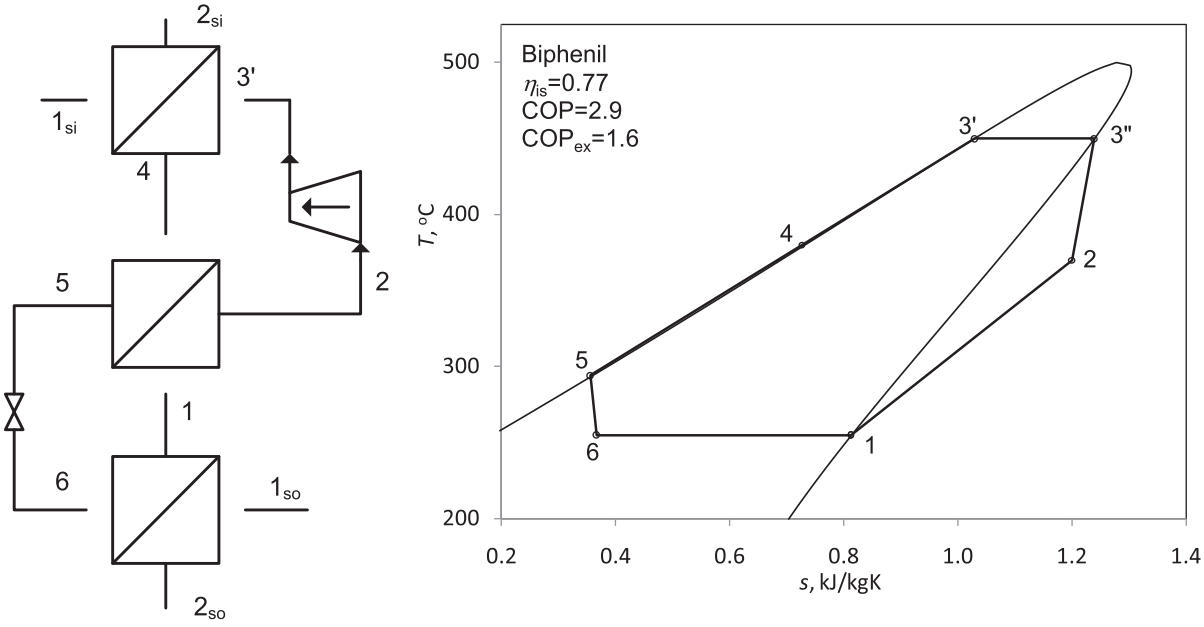

Fig. 23 – Heat pump configuration and phase diagram of biphenyl heat pump.

plants, such as disruption to heat supply due to nuclear plant outage.

Alternatively, heat pumps could further upgrade the waste heat, either by chemical heat pumps that release heat at successively higher temperatures in exothermic reactors (i.e., salt/ammonia or MgO/vapor chemical heat pumps), or vapor compression heat pumps [38–42]. A CuCl vapor compression heat pump is illustrated in Fig. 22. It uses CuCl as a cycle working fluid and heat pump fluid simultaneously. High coefficients of performance (COP) above 10 have been predicted with direct contact heat exchangers, using internal heat recovery with a CuCl heat pump [43].

Organic and titanium based working fluids for high temperature heat pumps have also been investigated. High COPs above 7 can be obtained by two-phase compression and internal heat recovery with retrograde organic working fluids. Biphenyl, biphenylmethane, naphthalene, isoquinoline, titanium-tetrabromide and titanium-tetraiodide have been investigated. Thermodynamic T-s diagrams and equations of state were developed. A conceptual cycle configuration and T-s diagram with internal heat recovery in a biphenyl heat pump is illustrated in Fig. 23. These types of high temperature heat pumps can allow temperature upgrading to higher levels from waste heat to supply thermal energy requirements of endothermic reactors in the Cu–Cl cycle. Promising results with high COPs have been obtained from a number of parametric studies of these heat pumps [40,41].

3.5. *Linkage of hydrogen and nuclear plants*

A Generation IV nuclear reactor, SCWR (Super-Critical Water Reactor) is being designed by AECL to operate at higher temperatures (up to 625 °C) that can facilitate co-generation of electricity and hydrogen. SCWR is expected to be able to co-generate electricity and hydrogen uniformly throughout the year, independently of the electrical load. With an electrical load decrease, the SCWR could produce more hydrogen and vice versa. Using high temperature heat from a nuclear power plant to heat water–steam in the hydrogen production loop is a promising option with SCWR. Heat exchangers of a recuperator-type would be used for this purpose (see Fig. 24). Currently, UOIT is collaborating with AECL on various plant configurations for co-generation of electricity and hydrogen [43–48].

3.6. *Safety and reliability*

Collaboration between UOIT and the University of Western Ontario, Canada, is investigating the reliability, fault diagnosis and probabilistic safety assessments of a nuclear hydrogen plant under various risk scenarios. Risk levels of a thermochemical Cu–Cl plant under different accident scenarios were analyzed by Zhang et al. [49]. Based on the results, potential problems encountered in the Cu–Cl cycle were identified and solutions recommended for future improvements.

Ma and Jiang [50,51] presented fault detection and isolation techniques for the power plant components. Sun

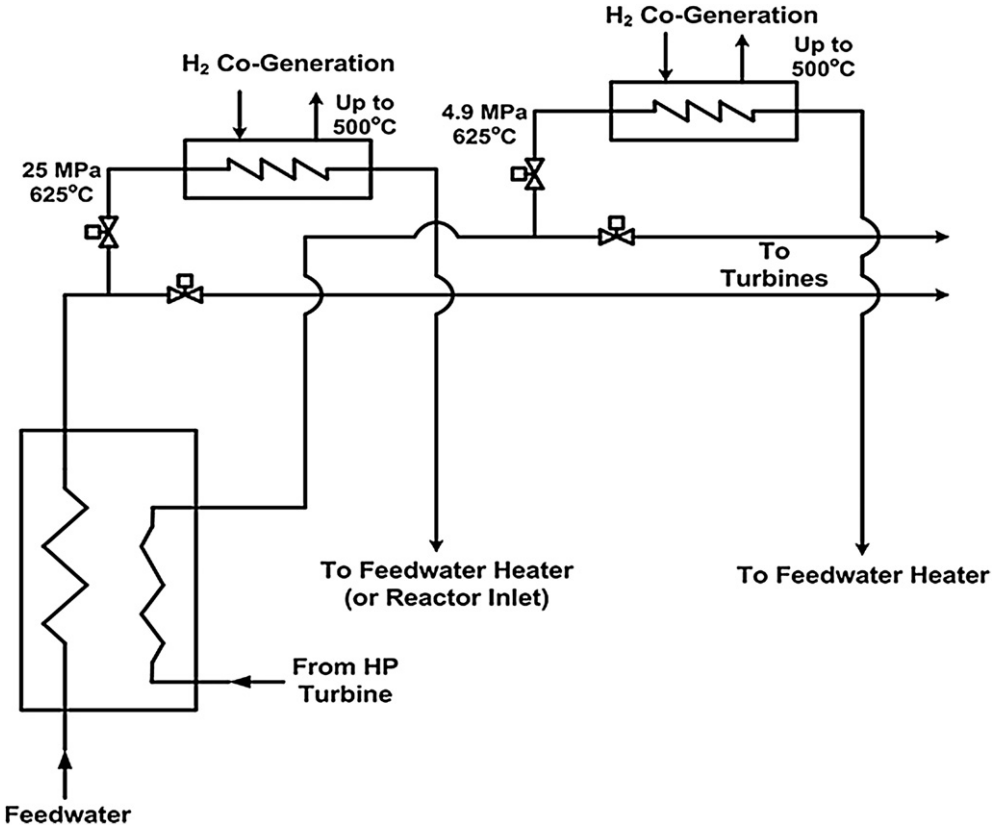

Fig. 24 – Single-reheat cycle with co-generation of hydrogen in a nuclear power plant.

and Jiang [52] performed modeling and simulation studies of the dynamic characteristics of SCWR. Al-Dabbagh and Lu [53,54] developed a distributed control system design for a nuclear hydrogen plant operating on the Cu–Cl cycle. The aim of these studies has been to develop control systems and safety precautions for various risk scenarios encountered in commercial operation of a nuclear hydrogen plant.

4. Thermochemistry and physical properties of working fluids

4.1. *Chemical potentials and solubility data*

Limited thermochemical data is available for the working fluids in the Cu–Cl cycle. Recent advances at UOIT have developed a new molecular-level simulation methodology to predict such data. The approach can either be used directly, or the simulation results can be fitted to standard empirical expressions and used in chemical process simulators. The methodology has been developed [55] to directly predict solubility data, in addition to chemical potentials, of electrolytes in aqueous solvents, using a molecular-level force-field model for the underlying system components. A description of the approach to calculate the solubilities and chemical potentials of aqueous electrolytes involving CuCl and $CuCl_2$ has been reported by Jirsak et al. [56]. The method incorporates multiple reactions involving the ionic complexes, and is based on the use of charged-Lennard-Jones potentials for the monatomic ions, whose parameters are obtained by fitting to experimental data. For the ionic complexes, the monatomic ions are used as building blocks, and the structures are determined by quantum mechanical approaches.

4.2. *Formation of Cu(I) and Cu(II) complexes*

Related studies have determined the equilibrium constants associated with Cu(I) and Cu(II) complexation with chloride ions as a function of temperature. These are being combined with literature values of complexation constants to yield a thermodynamic database for the copper-chloride–water system, in order to improve OLI and Aspen solubility

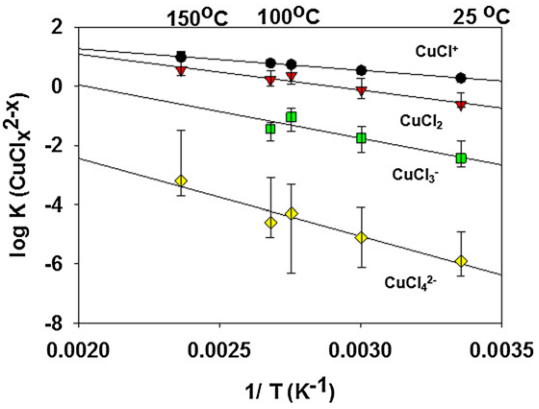

Fig. 25 – Complexation equilibrium constants.

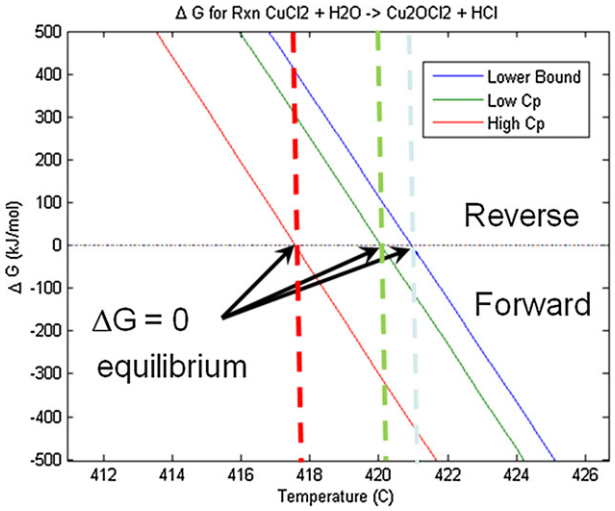

Fig. 26 – Gibbs free energy for reaction of copper oxychloride production.

calculations and electrochemical modeling capability. The thermodynamic data for the formation of Cu(I) and Cu(II) chloride species is crucial for improving the performance of the CuCl/HCl electrolysis cell. Cumulative formation constants of Cu_2(II) (aq) complexes with Cl^- (aq) were determined by a Principal Component Analysis of UV-spectra, obtained over a wide range of solution compositions and temperatures, coupled with a model for activity coefficients of the solution species. Fig. 25 illustrates measurements by Trevani et al. [57] and Ehlerova [58] for complexation equilibrium constants for $CuCl_x$ compounds. Shortcomings in the existing database are being addressed with extensions of past studies to higher temperatures and copper concentrations.

4.3. *Properties of copper oxychloride*

Thermochemical properties of copper oxychloride (not available elsewhere in archival literature) have also been investigated by Ikeda and Kaye [59]. Studies have been conducted to predict the interactions between metals, copper oxychloride and its decomposition products. Existing data for $CuCl_2$ and CuO is being used to predict the specific heat capacity (as a function of temperature) for copper oxychloride. This specific heat capacity was then used to determine the chemical free energy for the reaction to form (or decompose) the copper oxychloride. Fig. 26 illustrates the predicted free energy as a function of temperature for the decomposition reaction to produce copper oxychloride in the hydrolysis reaction. Temperatures higher than 400 °C will be avoided due to chlorine formation.

4.4. *Properties of Cu(I) and Cu(II) chloride*

Predictions and measurements of thermophysical properties of other copper/chlorine compounds have also been investigated [60–62]. This includes Cu(I) and Cu(II) chloride, cupric oxide, among others. The objective has been to develop an extensive and reliable database of thermophysical properties for all relevant Cu/Cl compounds for modeling, design and Aspen Plus

simulations, as well as potential byproducts from incomplete reactions in the Cu–Cl cycle.

Zamfirescu et al. [61] have developed new regression formulae to correlate the specific heat, enthalpy, entropy, Gibbs free energy, density, formation enthalpy and free energy of Cu(I) and Cu(II) chloride. Insufficient past literature data was available for the viscosity and thermal conductivity of molten CuCl, so new predictions were recently reported [61]. The properties were evaluated at 1 bar over a range of temperatures from ambient to 675–1000 K, which are consistent with the operating conditions of the Cu–Cl cycle. For molten CuCl, the estimated viscosity varies from 1.7 to 2.6 mPa s for the envisaged range of temperatures. A Riedel-like equation was developed for molten CuCl to correlate the vapor pressures with temperature.

5. Advanced materials

5.1. *Materials of construction for the CuCl/HCl electrolyzer*

Material degradation studies have been performed by AECL for selected materials under the expected operating conditions of the CuCl/HCl electrolyzer [11]. In the experiments, 24 selected materials were tested, including metals, ceramics, elastomers, polymers, carbon-based and composites. Each was exposed to operating conditions of 160 °C, 2.5 MPa and concentrated solutions of HCl, CuCl and $CuCl_2$. These include very aggressive conditions that accelerate the corrosion reactions. The electrolyzer requires a range of materials of construction, so a variety of materials have been tested. Glass-lined metal may be suitable as a material of construction, however it was found that glass may dissolve up to 0.7 mm/annum in aqueous conditions.

Ongoing research is also being performed at UOIT by Ranganathan and Easton [63], who have studied ceramic carbon electrodes (CCE) for the anode of the CuCl/HCl electrolysis cell. The CCE catalyst layer is a three-dimensional porous structure composed of carbon black and poly aminopropyl siloxane (PAPS). An SEM image of a CCE layer containing 36 wt% PAPS is shown in Fig. 27. These CCE layers were found to outperform bare CFP or graphite plates at low CuCl concentrations [63]. The superior electrode performance was attributed to the CCE's higher carbon surface area and greatly enhanced transport of anionic Cu(I) species arising from the presence of PAPS in its protonated form. More recent experiments have examined the CCE performance at higher concentrations of CuCl. More recent experiments have examined the CCE performance at higher concentrations of CuCl [74]. Fig. 28 compares the anodic polarization curves obtained with CCEs to that obtained with a bare CFP (carbon fiber paper) electrode in a solution containing 0.5 M CuCl in 6 M HCl. A clear performance advantage is retained at high CuCl concentrations that closely mimic the targeted cell operating conditions.

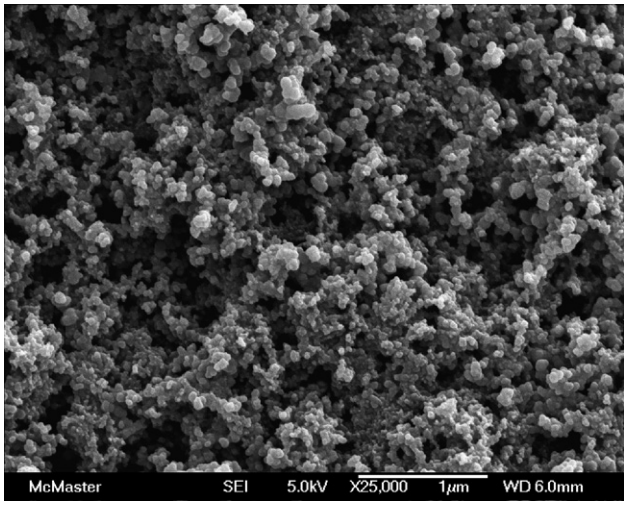

Fig. 27 – SEM image of a CCE anode catalyst layer containing 36 wt% PAPS.

5.2. *Corrosion resistant nickel alloy coatings*

Nickel alloy coatings are also being developed for corrosion resistance against high temperature Cu(I) chloride and HCl environments (exiting hydrolysis reactor) in the Cu–Cl cycle. Experimental studies have evaluated various surface coatings using electrochemical impedance spectroscopy (EIS). The corrosion performance of specimens is tested by immersing coupons in different CuCl/HCl environments. Fig. 29 shows a schematic of the immersion cell apparatus. An HCl cylinder (1) supplies a test cell (3) containing CuCl and the specimen. A heater (2) is used to melt the CuCl and control the temperature of the experiment. Items 4 and 5 are the exhaust and scrubber systems to control the release of the noxious fumes.

A potentiostat is used to control the voltage of the test specimen in the cell by passing current through the electrolyte. The working electrode potential is monitored using an Ag/AgCl reference electrode (see Fig. 30). A small AC signal is added to the control signal, and the phase and amplitude of the current response are measured. By comparing the AC voltage input and the AC current response, an impedance for the system is determined. By removing oxygen from the electrolyte, using an inert electrolyte system, and maintaining a base electrode potential in an inactive (non-corroding) range, the impedance of the metal/coating/interface system can be determined in the absence of a corrosion reaction.

Impedance spectra of uncoated and coated Inconel 625 specimens are shown in Figs. 31 and 32. It was found that Inconel 625 has a higher imaginary impedance (Z", vertical axis) and resistance (real impedance, Z', horizontal axis) than Al6XN stainless steel (not shown), suggesting that the naturally formed Inconel film is more protective than the film on Al6XN (smaller impedance). The impedance is inversely proportional to capacitance, and the capacitance is inversely proportional to the film thickness, so the higher impedance suggests a thicker film. The impedance data was numerically fitted to a variety of equivalent passive-electric circuits. The best fit was obtained in Figs. 31 and 32. The circuit element *Rs* was the solution resistance, *Rf* was designated as the film resistance and *Cf* was designated as the film capacitance. The result of the best fit circuit was obtained when a CPE element

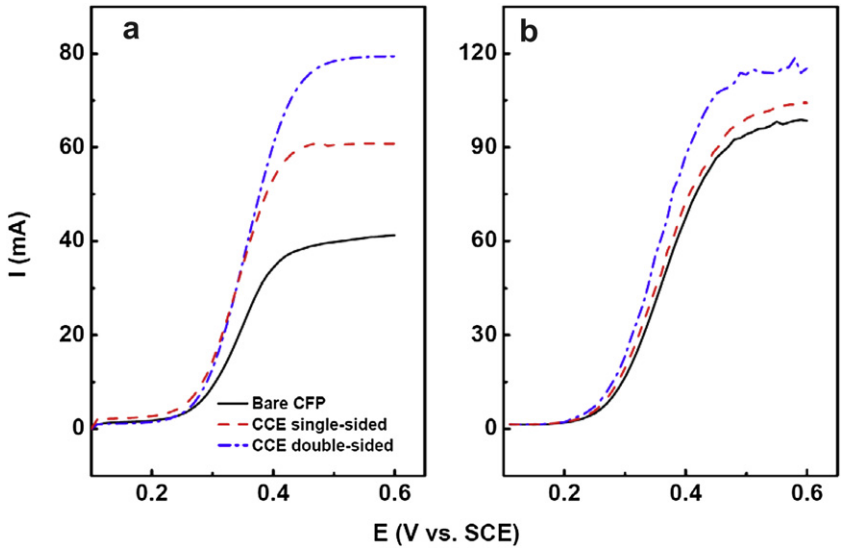

Fig. 28 – Comparison of anodic polarization curves obtained with bare CFP and CCE catalyst layers under (a) quiescent conditions and (b) with the solution stirred at 380 RPM (note: measurements at 25 °C using 0.5 M CuCl dissolved in 6 M HCl) [74].

(constant phase element) included non-ideal capacitance effects such as surface roughness.

The effects of a coating on the impedance response of Inconel 625 are shown in Fig. 32. The coating now dominates the impedance response, replacing the natural passive layer as the important conduction path from the solution to the metal. The new best fit circuit shown below the figure contains a resistor across the CPE element. Coating the Al6XN specimen changed the shape of the impedance plot in the same way as observed for the Inconel uncoated-to-coated specimens. The Z" change was not as dramatic as observed for Inconel (7500–6500 Ω), but the resistance nearly doubled. This may indicate that the quality of the coating has not changed much from the Al6XN base oxide, but the effective thickness of the layer has increased. The best circuit fit found for the Al6XN coated specimen was the same as the circuit for the coated Inconel specimen, indicating that both impedance measurements were interrogating the same type of film.

6. Economics and commercial transition to hydrogen economy

6.1. *Economics of nuclear hydrogen production*

A case study of distributed hydrogen production by electrolysis was presented by Miller [64,65], for hydrogen vehicles supplied by neighborhood fueling stations. Naterer et al. [66] compared electrolysis against SMR (steam–methane reforming) and thermochemical production of hydrogen with the Cu–Cl cycle. Thermochemical Cu–Cl plant costs were estimated by Orhan et al. [27], assuming a 15%/year return on

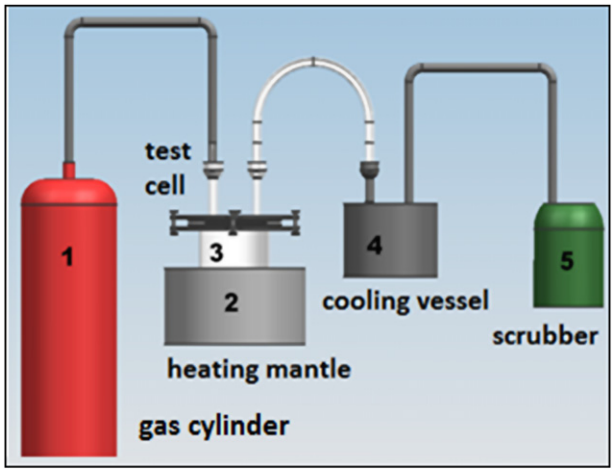

Fig. 29 – Schematic of immersion cell apparatus for working fluids in Cu–Cl cycle.

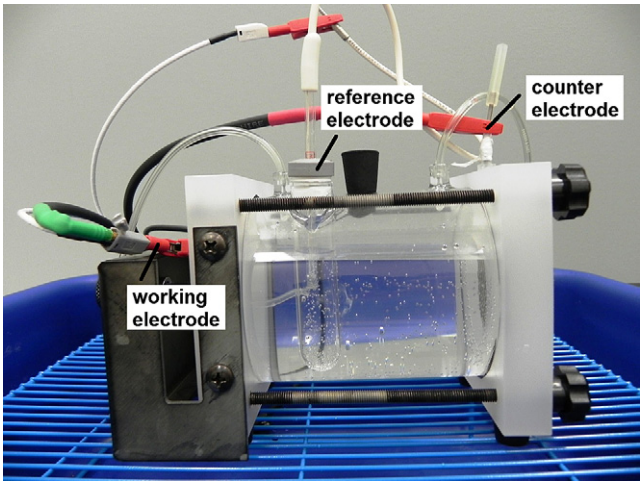

Fig. 30 – Electrochemical cell for corrosion testing.

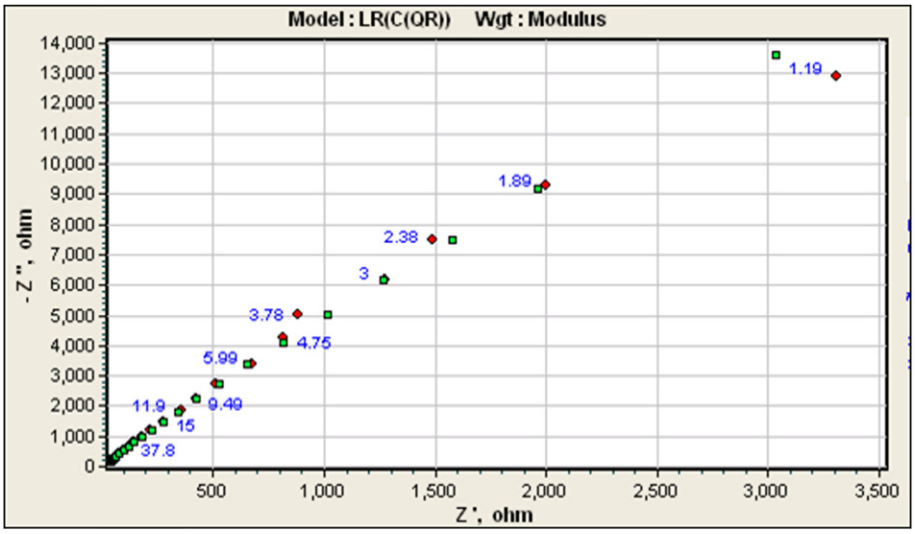

Fig. 31 – Impedance spectra for Inconel 625.

investment and a 10-year amortization, which is approximately equivalent to an annual capital charge of 20%. A production cost of $300/kW for the electrolysis cells was assumed, along with storage costs of $800,000/tonne of hydrogen via tube storage. Cost comparisons by Naterer et al. [66] were made against this benchmark case reported by Miller [65], for centralized production of hydrogen, based on SMR and a thermochemical copper–chlorine (Cu–Cl) cycle linked with a nuclear reactor, or natural gas heating to supply the high-grade heat requirements of the thermochemical cycle. Below capacities of between about 10 and 20 tonnes/day, electrolysis from off-peak electricity was shown to have a lower unit cost of hydrogen production, although the advantage reverses at higher capacities. Electrolysis costs can take advantage of off-peak electricity, so an analogous benefit could be realized with a Cu–Cl cycle linked with SCWR. For example, a certain base-load production of hydrogen can be maintained with SCWR, but a bypass heat exchanger could redirect steam from the power turbine to the Cu–Cl plant during off-peak periods of low electricity demand [66].

6.2. *Electrolysis vs. thermochemical hydrogen production*

The emerging Hydrogen Economy will need an integrated group of sustainable technologies for hydrogen production, including thermochemical water splitting, high temperature electrolysis, conventional water electrolysis and other hybrid methods. These technologies will likely complement, not compete against, one another. Electrolysis, for example, allows for de-centralized production of hydrogen (at perhaps a remote wind or solar power facility, or at the point of sale) and the generation of hydrogen during off-peak hours at power plants, when electricity prices and demand are lowest.

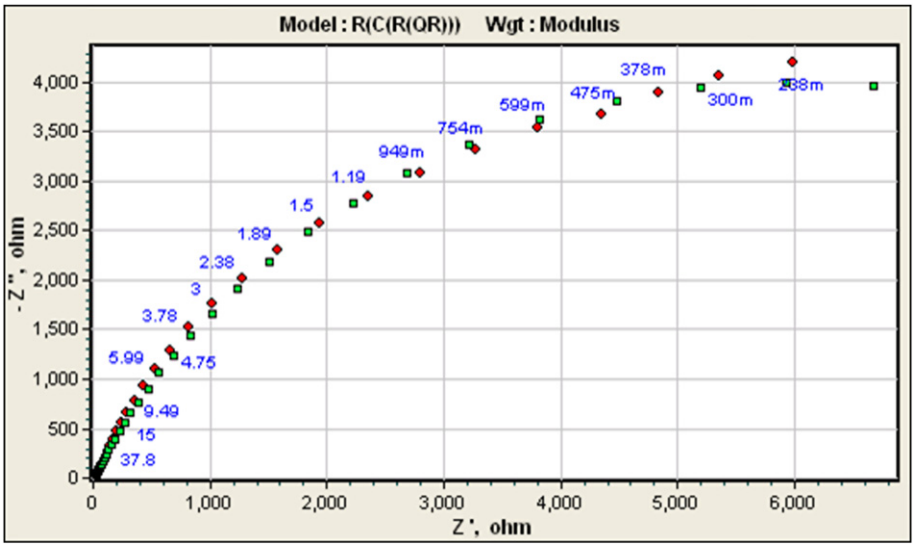

Fig. 32 – Impedance spectra for Diamalloy 4006 coated Inconel 625.

Thermochemical cycles, by comparison, are much more efficient emerging technologies that can integrate well with electrolysis because they allow for centralized, base-load production of hydrogen, and the utilization of waste heat from power plants. Thermochemical cycles have the potential to be much more efficient than electrolysis when associated with nuclear power because there is no need for generation of electricity from the process heat (which encounters a significant energy loss). Naterer et al. [67,68] examined how the integration of these technologies can lead to reduced cost and environmental impact of hydrogen production.

The use of hydrogen as an energy carrier is appealing from the perspective of electrical grid management, because of its energy storage potential. The use of hydrogen as an energy carrier can increase the efficiency and reliability of the electric grid. When integrated into the electrical power distribution system, hydrogen can become a major solution to the electricity storage issue, facilitating the increased use of intermittent renewable energy sources such as wind and solar, while maintaining the necessary reliability and consistency of the electrical grid.

Near-term clean production of hydrogen is likely to be associated with electrolysis to support and enable intermittent renewable power sources, as well as load leveling of base-load power sources, such as nuclear plants. From the electrical grid management point of view, the use of hydrogen as an energy carrier is appealing in the context of energy storage impact on competitive electricity markets. It enables power utilities to take advantage of significant price differences between peak and off-peak pricing hours (which may or may not necessarily coincide with peak and off-peak demand hours). Ancillary services such as voltage and frequency regulation are those services necessary to support the transmission of electric power from seller to purchaser, while maintaining reliable operations of the interconnected transmission system. Some of these services require a "spinning reserve", where generation reserve capacity may be called shortly after an event that causes significant deviation from the standard voltage and frequency of the grid. This service requires a payment to the generator that is ready to increase/reduce power when requested. Water electrolysis as a variable and controllable load has the potential to address this market need in the short term. However, this only represents a fraction of the required hydrogen for the emerging hydrogen economy, so larger scale production via thermochemical plants will become increasingly important.

6.3. *Hydrogen transition in the transportation sector*

Hajimiragha et al. [68] investigated the implementation of electrolytic hydrogen production for Ontario's transportation sector, based on its existing electricity system infrastructure and planned future development up to 2025. Using a zonal based model of Ontario's electricity transmission network and Ontario's Integrated Power System Plan (IPSP), a pattern of generation capacity procurement in Ontario from 2008 to 2025 was presented. A model was also developed to find the optimal size of hydrogen production plants in different zones, as well as optimal hydrogen transportation routes for a significant hydrogen economy penetration in Ontario by 2025. The results indicate that the present and projected electricity supply in Ontario can achieve significant levels of hydrogen penetration in the transportation sector by 2025, without additional grid or power generation infrastructure beyond those currently planned. The study showed that up to 1.2% of the current light duty vehicle fleet (over 100,000 vehicles) can be supported within this period, however beyond this time frame with increased penetration of hydrogen vehicles, large-scale hydrogen production will be required. Nevertheless, even with this limited penetration of hydrogen vehicles, Kantor et al. [69] have shown that there would be measurable impact on urban air quality in Ontario.

Although much attention has focused on hydrogen fuel cell vehicles for the automotive sector, several studies have shown that hydrogen may be more advantageous and economical for passenger trains. Of all transportation modes, train and marine transport may be the most attractive entry points for the Hydrogen Economy [70]. Rail transport is more efficient than trucks for long-range transport and it has better opportunities for expansion. Hydrogen for airplanes is also feasible and attractive, although the aircraft industry is conservative, requires long lead times for major design changes, and aircraft designs would need significant re-configurations to accommodate the volume of liquid hydrogen.

Recent studies by Haseli et al. [71] and Marin et al. [72,73] have examined the environmental impact and feasibility of hydrogen vs. electrification as a cleaner alternative to diesel locomotives in Ontario, Canada. Disadvantages of electrification include the capital investment to install electrical substations and catenaries, together with lack of flexibility for trains to move into other service areas not covered by electrification. Marin et al. [72,73] analyzed the implementation and operation of hydrogen passenger locomotives (fueled by nuclear-produced hydrogen) in the GO Transit Lakeshore corridor, between Oshawa and Toronto, Ontario. A sensitivity analysis was performed over a range of operational costs for a hydrogen train, with variability of feedstock prices, fuel cell power density and expected return on capital investment. Various methods of propulsion and storage were compared against electrification. It was found that hydrogen trains offer a number of environmental, technical and economic benefits over electrification and other modes of transportation, specifically through a case study for Ontario, Canada.

7. Conclusions

This paper has presented the recent Canadian advances in nuclear-based hydrogen production, particularly involving the thermochemical Cu–Cl cycle and electrolysis. The Cu–Cl cycle was identified by Atomic Energy of Canada Limited, AECL (CRL; Chalk River Laboratories), as the most promising cycle for thermochemical hydrogen production with the Generation IV nuclear reactor, SCWR (Super-Critical Water Reactor). Objectives of Canada's nuclear hydrogen program are to develop commercially viable processes for producing hydrogen based on the thermochemical Cu–Cl cycle and water electrolysis. In collaboration with the Argonne National Laboratory, this would ultimately achieve the DOE cost target ($3 gge) and efficiency target (>35% based on LHV) for nuclear hydrogen production.

The Cu–Cl cycle has attractive features that should help to meet these targets, particularly a 530 °C maximum temperature that reduces demands on materials, compared to higher temperature cycles. Also, the Cu–Cl cycle couples well with various heat sources, such as the SCWR, solar power tower or Na-cooled fast reactor. The yields are nearly 100% in the hydrolysis and copper oxychloride decomposition processes, without catalysts and no recycle streams in these reactions. Also, conceptual process designs use commercially practiced processes in industry. The hydrogen production costs are therefore believed to be within the range of DOE targets.

Acknowledgements

Support of this research and assistance from Atomic Energy of Canada Limited, Ontario Research Excellence Fund, Argonne National Laboratory (International Nuclear Energy Research Initiative; U.S. Department of Energy), Natural Sciences and Engineering Research Council of Canada (NSERC), University Network of Excellence in Nuclear Engineering (UNENE) and the Canada Research Chairs (CRC) program are gratefully acknowledged.

REFERENCES

[1] Naterer GF, Suppiah S, Lewis M, Gabriel K, Dincer I, Rosen MA, et al. Recent Canadian advances in nuclear-based hydrogen production and the thermochemical Cu–Cl cycle. International Journal of Hydrogen Energy 2009;34:2901–17.

[2] Stevens MB, Fowler MW, Elkamel A, Elhedhli S. Macro-level optimized deployment of an electrolyser-based hydrogen refuelling infrastructure with demand growth. Engineering Optimization 2008;40(10):955–67.

[3] McQuillan BW, Brown LC, Besenbruch GE, Tolman R, Cramer T, Russ BE, et al. High efficiency generation of hydrogen fuels using solar thermochemical splitting of water. Annual report, GA-A24972. San Diego, CA: General Atomics; 2002.

[4] Lewis M, Taylor A. High temperature thermochemical processes. DOE hydrogen program. Annual progress report. Washington, DC; 2006. p. 182–85

[5] Sakurai M, Nakajima H, Amir R, Onuki K, Shimizu S. Experimental study on side-reaction occurrence condition in the iodine–sulfur thermochemical hydrogen production process. International Journal of Hydrogen Energy 2000;23: 613–9.

[6] Schultz K. Thermochemical production of hydrogen from solar and nuclear energy. Technical report for the Stanford global climate and energy project. San Diego, CA: General Atomics; 2003.

[7] Sadhankar RR, Li J, Li H, Ryland D, Suppiah S. Hydrogen generation using high-temperature nuclear reactors. In: 55th Canadian chemical engineering conference, Toronto, Ontario; October, 2005.

[8] Carty RH, Mazumder M, Schreider JD, Panborn JB. GRI Report 80-0023. Thermochemical hydrogen production, vol. 1. Chicago, IL 60616: Gas Research Institute for the Institute of Gas Technology; 1981.

[9] Lewis MA, Masin JG, Vilim RB, Serban M. Development of the low temperature Cu–Cl thermochemical cycle. In: International congress on advances in nuclear power plants, Seoul, Korea; May 15–19, 2005.

[10] Xiao ZF, Gammons CH, Williams-Jones AE. Experimental study of copper(I) chloride complexing in hydrothermal solutions at 40 to 300 °C and saturated water vapor pressure. Geochimica et Cosmochimica Acta 1998;62:2949–64.

[11] Suppiah S, Naterer GF, Lewis M, Lvov S, Easton B, Dincer I, et al. Thermo-mechanical design of nuclear-based hydrogen production. In: ORF workshops on nuclear-based thermochemical hydrogen production, Oshawa, ON (December 2007, May 2009, February 2010) and Chalk River, ON (October 2008).

[12] Naterer GF, Daggupati V, Marin G, Gabriel K, Wang Z. Thermochemical hydrogen production with a copper–chlorine cycle, II: flashing and drying of aqueous cupric chloride. International Journal of Hydrogen Energy 2008;33:5451–9.

[13] Bahadorani P, Naterer GF, Gabriel K. Effects of cupric chloride concentration on aqueous droplet evaporation in the Cu–Cl cycle. In: International conference on hydrogen production, Oshawa, Ontario; May 3–6, 2009.

[14] Bahadorani P, Naterer GF, Gabriel K. Particle formation from slurry spray drying in nuclear-based hydrogen production. In: International conference on hydrogen and fuel cells, Vancouver, British Columbia; May 31–June 3, 2009.

[15] Daggupati V, Naterer GF, Gabriel K. Diffusion of gaseous products through a particle surface layer in a fluidized bed reactor. International Journal of Heat and Mass Transfer 2010;53:2449–58.

[16] Daggupati V, Naterer GF, Gabriel K, Gravelsins R, Wang Z. Equilibrium conversion in Cu–Cl cycle multiphase processes of hydrogen production. Thermochimica Acta 2009;496: 117–23.

[17] Daggupati V, Naterer GF, Gabriel K, Gravelsins R, Wang Z. Decomposition analysis of cupric chloride hydrolysis in the Cu–Cl cycle of hydrogen production. In: International conference on hydrogen production, Oshawa, Ontario; May 3–6, 2009.

[18] Daggupati V, Naterer GF, Gabriel K. Reaction rate analysis of cupric chloride hydrolysis for production of hydrogen in a copper–chlorine thermochemical cycle. In: National hydrogen association conference, Columbia, SC; March 30–April 3, 2009.

[19] Serban M, Lewis MA, Basco JK, Kinetic study of the hydrogen and oxygen production reactions in the copper-chloride thermochemical cycle. In: AIChE 2004 spring national meeting, New Orleans, LA; April 25–29, 2004.

[20] Jaber O, Naterer GF, Dincer I. Heat recovery from molten CuCl in the Cu–Cl cycle of hydrogen production. International Journal of Hydrogen Energy June 2010;35(12):6140–51.

[21] Ghandehariun S, Naterer GF, Rosen MA, Wang Z. Options for heat recovery from molten salt in thermochemical hydrogen production. In: CSME Forum 2010, Victoria, BC; June 7–9, 2010.

[22] Ferrandon MS, Lewis MA, Tatterson DF, Nankanic RV, Kumarc M, Wedgewood LE, et al. The hybrid Cu–Cl thermochemical cycle. I. Conceptual process design and H_2A cost analysis. II. Limiting the formation of CuCl during hydrolysis. In: NHA annual hydrogen conference, Sacramento convention center, CA; March 30–April 3, 2008.

[23] Chukwu C, Naterer GF, Rosen MA. Process simulation of nuclear-produced hydrogen with a Cu–Cl Cycle. In: 29th Conference of the Canadian nuclear society, Toronto, Ontario; June 1–4, 2008

[24] Wang ZL, Naterer GF, Gabriel KS, Gravelsins R, Daggupati VN. New Cu–Cl thermochemical cycle for hydrogen production with reduced excess steam requirements. International Journal of Green Energy 2009;6:616–26.

[25] McDougall R, Nokleby SB. Multi-objective parallel asynchronous particle swarm optimization for engineering design problems. In: ASME international design engineering technical conferences, San Diego, CA; August 30–September 2, 2009.
[26] Orhan MF, Dincer I, Rosen MA. Thermodynamic analysis of the copper production step in a copper–chlorine cycle for hydrogen production. Thermochimica Acta 2008;480(1–2): 22–9.
[27] Orhan MF, Dincer I, Naterer GF. Cost analysis of a thermochemical Cu–Cl pilot plant for nuclear-based hydrogen production. International Journal of Hydrogen Energy 2008;33:6006–20.
[28] Orhan MF, Dincer I, Rosen MA. The oxygen production step of a copper–chlorine thermochemical water decomposition cycle for hydrogen production: energy and exergy analyses. Chemical Engineering Science 2009;64:860–9.
[29] Rosen MA. Advances in hydrogen production by thermochemical water decomposition: a review. Energy 2010;35(2):1068–76 [invited].
[30] Orhan MF, Dincer I, Rosen MA. Energy and exergy analyses of the fluidized bed of a copper–chlorine cycle for nuclear-based hydrogen production via thermochemical water decomposition. Chemical Engineering Research and Design 2009;87:684–94.
[31] Orhan MF, Dincer I, Rosen MA. Energy and exergy analyses of the drying step of a copper–chlorine thermochemical cycle for hydrogen production. International Journal of Exergy 2009;6:793–808.
[32] Orhan MF, Dincer I, Rosen MA. Energy and exergy assessments of the hydrogen production step of a copper–chlorine thermochemical water splitting cycle driven by nuclear-based heat. International Journal of Hydrogen Energy 2008;33(22):6456–66.
[33] Lubis LL, Dincer I, Rosen MA. Life cycle assessment of hydrogen production using nuclear energy: an application based on thermochemical water splitting. Journal of Energy Resources Technology 2010;132(2):021004 (6 pages).
[34] Solli C, Stromman AH, Hertwish EG. Fission or fossil: life cycle assessment of hydrogen production. Proceedings of the IEEE 2006;94(10).
[35] Utgikar V, Thiesen T. Life cycle assessment of high temperature electrolysis for hydrogen production via nuclear energy. International Journal of Hydrogen Energy 2006;31:939–44.
[36] Goedkoop M, Demmers M, Collignon M. The eco-indicator 95 manual for designers. National reuse of waste research programme, Netherlands; 1996
[37] Spekkens P, Naterer GF, Gravelsins R, Wang F, Secnik E. Personal communication. Pickering, Ontario, Canada: Ontario Power Generation; March, 2010.
[38] Granovskii M, Dincer I, Rosen MA, Pioro I. Thermodynamic analysis of the use of a chemical heat pump to link a super-critical water-cooled nuclear reactor and a thermochemical water-splitting cycle for hydrogen production. JSME Journal of Power and Energy Systems 2008;2:756–67.
[39] Naterer GF. Second law viability of upgrading industrial waste heat for thermochemical hydrogen production. International Journal of Hydrogen Energy 2008;33:6037–45.
[40] Zamfirescu C, Dincer I, Naterer GF. Performance evaluation of organic and titanium based working fluids for high temperature heat pumps. Thermochimica Acta 2009;496: 18–25.
[41] Zamfirescu C, Naterer GF, Dincer I. Upgrading of waste heat for combined power and hydrogen production with nuclear reactors. ASME Journal of Engineering for Gas Turbines and Power October, 2010;132(10):102911–9.
[42] Zamfirescu C, Naterer GF, Dincer I. Coupled CuCl heat pump and endothermic oxy-decomposer for sustainable hydrogen generation. In: Renewable hydrogen national symposium, Winnipeg, Manitoba; January 18–29, 2010.
[43] Naidin M, Mokry S, Baig F, Gospodinov Ye, Zirn U, Pioro I, et al. Thermal-design options for pressure-channel SCWRs with co-generation of hydrogen. Journal of Engineering for Gas Turbines and Power January, 2009;131.
[44] Naidin M, Pioro I, Duffey R, Mokry S, Grande L, Villamere B, et al. Super-critical water-cooled nuclear reactors (SCWRs): thermodynamic cycle options and thermal aspects of pressure-channel design. In: International conference on opportunities and challenges for water cooled reactors in the 21st century. Book of extended synopses. Vienna, Austria: IAEA; 2009. p. 134–5. Oct. 27–30, Paper 5S03.
[45] Naidin M, Monichan R, Zirn U, Gabriel K, Pioro I. Thermodynamic considerations for a single-reheat cycle SCWR. In: Proceedings of the 17th international conference on nuclear engineering (ICONE-17), Paper #75984, Brussels, Belgium; July 12–16, 2009.
[46] Naidin M, Mokry S, Monichan R, Chophla K, Pioro I, Naterer G, et al. Thermodynamic analysis of SCW NPP cycles with thermo-chemical co-generation of hydrogen. In: Proceedings of the international conference on hydrogen production-2009 (ICH2P-09), Paper No. ICH2P-GP163, Oshawa, Ontario, Canada; May, 2009.
[47] Wang Z, Naterer GF, Gabriel K. Thermal integration of SCWR nuclear and thermochemical hydrogen plants. In: 2nd Canada–China joint conference on super-critical water-cooled reactors, Toronto, ON; April 25–28, 2010.
[48] Wang F, Naterer GF, Gabriel K, Gravelsins R, Daggupati V. Coupling of nuclear heat to hydrogen production thermochemical cycles, Paper ICONE 17-75702. In: ASME 17th international conference on nuclear engineering, Brussels, Belgium; July 12–16, 2009.
[49] Zhang Y, Lu L, Naterer GF. Reliability and safety assessment of a conceptual thermochemical plant for nuclear-based hydrogen generation. In: ASME 16th international conference on nuclear engineering, Orlando, Florida; May 11–15, 2008.
[50] Ma J, Jiang J. Applications of fault diagnosis in nuclear power plants: an introductory survey. In: Proceedings of the 7th IFAC symposium on fault detection, supervision and safety of technical processes (SAFEPROCESS 2009), Barcelona, Spain; June 30–July 3, 2009. p. 1150–61.
[51] Ma J, Jiang J. A fault detection and isolation technique for in-core flux detectors. In: Proceedings of the sixth american nuclear society international topical meeting on nuclear plant instrumentation, control, and human-machine interface technologies (NPIC & HMIT 2009), Knoxville, Tennessee; April 5–9, 2009.
[52] Sun PW, Jiang J. Modelling and simulation of dynamic characteristics of CANDU-SCWR. In: 2nd Canada–China joint workshop on super-critical water-cooled reactors, Toronto; April 25–28, 2010.
[53] Al-Dabbagh AW, Lu L. Design and reliability prediction of the control system for nuclear-based hydrogen production with copper–chlorine thermochemical cycle. International Journal of Hydrogen Energy 2010;35:966–77.
[54] Al-Dabbagh AW, Lu L. A distributed control system design for nuclear-based hydrogen production with copper–chlorine thermochemical cycle. In: Proceedings of the 30th annual conference of the Canadian nuclear society; 2009.
[55] Smith WR, Nezbeda I, Jirsak J, Skvor J. Molecular-level simulation of electrolyte systems in the Cu–Cl hydrogen production cycle. In: 8th World Congress on Chemical Engineering, Montreal, QC; Aug 23–27, 2009.
[56] Jirsak J, Skvor J, Smith WR, Nezbeda I. Molecular-level simulation of electrolyte system solubility and chemical speciation. In: DECHEMA workshop on molecular modeling

and simulation for industrial applications, Wurzburg, Germany; Mar. 22–23, 2010.
[57] Trevani L, Ehlerova J, Sedlbauer J, Tremaine PR. Complexation in the Cu(II)–LiCl–H_2O system at temperatures to 423 K by UV–visible spectroscopy. In: International Journal of Hydrogen Energy 2010;35(10): 4893–4900.
[58] Ehlerova J. Spectrophotometric determination of equilibrium constants and speciation of aqueous systems over a wide range of temperatures and pressures. PhD Thesis. Technical University of Liberec, Czech Republic; 2009
[59] Ikeda BM, Kaye MH. Thermodynamic properties in the Cu–Cl–O–H system. In: 7th International conference on nuclear and radiochemistry, Budapest, Hungary; August 2008.
[60] Avsec J, Naterer GF. Thermodynamic property evaluation of copper-chlorine fluid components at high temperatures. In: AIAA 40th thermophysics conference, Seattle, WA; June 23–26, 2008.
[61] Zamfirescu C, Dincer I, Naterer GF. Thermophysical properties of copper compounds in copper–chlorine thermochemical water splitting cycles. International Journal of Hydrogen Energy May 2010;35(10):4839–52.
[62] Avsec J, Naterer GF, Predin A. Calculation of thermodynamic properties for hydrochloric and copper compounds in a hydrogen production process. Journal of Energy Technology, in press.
[63] Ranganathan S, Easton EB. Ceramic carbon electrode-based anodes for use in the Cu–Cl thermochemical cycle. International Journal of Hydrogen Energy May 2010;35(10): 4871–6.
[64] Miller AI, Duffey RB. Sustainable and economic hydrogen co-generation from nuclear energy in competitive power markets. In: International energy workshop, Laxenburg, Austria; June 24–26, 2003.
[65] Miller AI. Electrochemical production of hydrogen by nuclear energy. Nuclear production of hydrogen – technologies and perspectives for global deployment. La Grange Park, Illinois: American Nuclear Society; 2004 [Chapter 4].
[66] Naterer GF, Fowler M, Cotton J, Gabriel K. Synergistic roles of off-peak electrolysis and thermochemical production of hydrogen from nuclear energy in Canada. International Journal of Hydrogen Energy 2008;33:6849–57.
[67] Naterer GF, Jaber O, Dincer I. Environmental impact comparison of steam methane reformation and thermochemical processes of hydrogen production. In: 18th World hydrogen energy conference, Essen, Germany; May 16–21, 2010.
[68] Hajimiragha A, Fowler MW, Cañizares CA. Hydrogen economy transition in Ontario – Canada considering the electricity grid constraints. International Journal of Hydrogen Energy 2009;34(13):5275–93.
[69] Kantor I, Fowler MW, Hajimiragha A, Elkamel A. Air quality and environmental impacts of alternative vehicle technologies in Ontario, Canada. International Journal of Hydrogen Energy May 2010;35(10):5145–53.
[70] Miller A. Hydrail: an adaptable, low-cost alternative to electrification, Paper 4-205-4. In: Hydrogen and fuel cells conference, Vancouver, British Columbia; April 29–May 2, 2007.
[71] Haseli Y, Naterer GF, Dincer I. Comparative assessment of greenhouse gas mitigation of hydrogen passenger trains. International Journal of Hydrogen Energy 2008;33:1788–96.
[72] Marin G, Naterer GF, Gabriel KS. Rail transportation by hydrogen vs. electrification – case study for Ontario Canada, I: propulsion and storage. International Journal of Hydrogen Energy 2010;35:6084–96.
[73] Marin G, Naterer GF, Gabriel KS. Rail transportation by hydrogen vs. electrification – case study for Ontario Canada, II: energy supply and distribution. International Journal of Hydrogen Energy 2010;35:6097–107.
[74] Ranganathan S, Easton EB. High performance ceramic carbon electrode-based anodes for use in the Cu–Cl thermochemical cycle for hydrogen production. International Journal of Hydrogen Energy 2010;35(3):1001–7.